Dark matter substructures affect dark matter-electron scattering in xenon-based direct detection experiments

Tarak Nath Maity[1] **and Ranjan Laha**[2]

Centre for High Energy Physics, Indian Institute of Science,
C. V. Raman Avenue, Bengaluru 560012, India

E-mail: tarak.maity.physics@gmail.com, ranjanlaha@iisc.ac.in

ABSTRACT: Recent sky surveys have discovered a large number of stellar substructures. It is highly likely that there are dark matter (DM) counterparts to these stellar substructures. We examine the implications of DM substructures for electron recoil (ER) direct detection (DD) rates in dual phase xenon experiments. We have utilized the results of the LAMOST survey and considered a few benchmark substructures in our analysis. Assuming that these substructures constitute $\sim 10\%$ of the local DM density, we study the discovery limits of DM-electron scattering cross sections considering one kg-year exposure and 1, 2, and 3 electron thresholds. With this exposure and threshold, it is possible to observe the effect of the considered DM substructure for the currently allowed parameter space. We also explore the sensitivity of these experiments in resolving the DM substructure fraction. For all the considered cases, we observe that DM having mass $\mathcal{O}(10)\,\mathrm{MeV}$ has a better prospect in resolving substructure fraction as compared to $\mathcal{O}(100)\,\mathrm{MeV}$ scale DM. We also find that within the currently allowed DM-electron scattering cross-section; these experiments can resolve the substructure fraction (provided it has a non-negligible contribution to the local DM density) with good accuracy for $\mathcal{O}(10)\,\mathrm{MeV}$ DM mass with one electron threshold.

---

[1]https://orcid.org/0000-0003-1069-6358.
[2]https://orcid.org/0000-0001-7104-5730.

Contents

1 Introduction

It is important to leave no stone unturned in the search for the DM identity. Numerous astrophysical and cosmological observations infer the irrefutable evidence of DM [1–4]. Despite these insurmountable evidences of the gravitational interaction of DM, we do not yet know if the DM candidate interacts via other forces. Numerous experiments have been performed to discover the non-gravitational signature of DM, but none of them have revealed a positive result. The DD experiments have been playing a pivotal role in their quest for the DM identity. The typical nuclear recoil (NR) DD experiments, searching for weak-scale DM, have made extraordinary progress [5–21]. Typical NR DD experiments lose their sensitivity due to kinematic mismatch for an incident non-relativistic ambient sub-GeV DM (see for instance [22–25]).[1] In order to fully characterize particle DM properties, it is important to probe DM-electron coupling too. A promising strategy to search for such DM interactions is to consider its scattering with electrons of the target materials [49–62]. In contrast with nuclear scattering, the maximum sensitivity to DM-electron interaction is

---

[1]Alternatively, one can boost non-relativistic light DM through scattering with energetic particles to overcome the threshold barrier, see for e.g., [26–34] or by utilizing the Migdal effect [35–45] or by absorption of fermionic DM (both for NR and ER) [46–48].

typically achieved at a lower DM mass. For e.g., assuming a xenon target and momentum independent scattering cross-section, the maximum sensitivity is achieved at $\sim 30\,\text{GeV}$ for DM-nuclear scattering and $\sim 200\,\text{MeV}$ for DM-electron scattering.

An ambient DM of mass $\mathcal{O}(10)\,\text{MeV}$ will have a kinetic energy of the $\mathcal{O}(10)\,\text{eV}$, which is in the ball-park of the atomic ionization energy or the band gap energy of semiconductor. This indicates that a sub-GeV DM can ionize an electron from an atomic shell or facilitate an electron's transition from the valance band to the conduction band. Many experiments like XENON [63], SuperCDMS [64], DarkSide-50 [65, 66], DAMIC [67], EDELWEISS [68], SENSEI [69, 70], PandaX-II [71] etc. are searching for the signatures of such a phenomenon.

The boundedness of electrons in the target material makes DM-electron scattering events inelastic. The DM velocity required to have a measurable recoil is rather high, which can be found near the tail of the DM velocity distribution (assuming that it has a Maxwell-Boltzmann form). These tails are quite sensitive to the choice of the DM velocity distribution [72–75]. The present DM velocity distribution depends on the galactic structure formation history. In the well-known paradigm of ΛCDM (Lambda Cold Dark Matter), bottom-up hierarchical structure formation is a generic feature [76–82]. Larger galaxies are formed from the merger of smaller galaxies (although the merger of similar mass galaxies may also lead to a bigger galaxy [83, 84]). The gravitational field of the Milky Way (MW) is non-uniform, and this non-uniformity gives rise to strong tidal forces. When smaller galaxies accrete into the MW galaxy, the gravitational force disrupts these galaxies resulting in tidal stripping of various components (including DM) of these infalling galaxies. For an ancient merger, the DM component will have time to virialize within the MW, which may lead to an isotropic, isothermal DM halo. This scenario is often referred to as the Standard Halo Model (SHM), with the Maxwell-Boltzmann distribution representing the DM distribution. However, for relatively recent mergers, there will not be sufficient time for virialization, resulting in plenty of substructures both in the stellar and in the DM component [85–97]. The presence of such additional stellar substructures (beyond the MW stars) have been detected by different sky-surveys like Gaia [83, 90, 97–100], SDSS [90], LAMOST [101, 102], etc., and have also been predicted in various N-body simulations [103–111].

Since these stellar substructures arise from merged galaxies, a DM counterpart must be associated with them too (because the DM is also present in the accreted galaxies before their merger). Whether DM would follow stellar distribution or not is a matter of debate. For example, the celestial part of the Sagittarius stream might not substantially overlap with the Solar neighborhood. However, the extended DM counterpart may overlap with our local position [112]. The similarities between DM and stellar distributions in debris flow have been pointed out in refs. [89, 113]. The dwarf spheroidals, which give rise to the S2-stream, are believed to have similar DM and stellar shape [114] before they merged with MW. Therefore the resemblance between stellar and DM substructures is not settled yet; more dedicated studies are needed to understand this. However, the presence of this DM might manifest in the local DM density and velocity distribution: this will result in a difference of the velocity distribution from the normal MB distribution with cut off at the galactic escape velocity [115, 116]. DM DD rate is strongly dependent on the local velocity distribution of DM [117–146], and a different DM velocity distribution can result in a large change

in our theoretical expectations. The effects of these substructures have been extensively studied in the literature in the context of typical NR DD experiments [114, 147–160]. This paper aims to study the effect of these DM substructures in the ER DM DD experiments assuming xenon-based detectors. Such a study has been conducted for semiconductor target material in ref. [73]. It was shown in ref. [75] that the effect of such astrophysical uncertainties is quite prominent for xenon targets. Further, in large regions of the DM parameter space, the sensitivity of xenon targets is a few orders of magnitude stronger than those from semiconductor-based experiments [63, 69–71] implying that xenon detectors will probably play a big role in discovering DM-electron scattering. These facts motivate our detailed study in this manuscript, where we highlight the importance of considering DM substructures while searching for DM-electron scattering.

It has been argued in refs. [83, 90, 92–94, 98, 99, 161] that there are plenty of stellar substructures in the local halo. We utilize the results of the LAMOST survey [101] to present the effect of the DM substructure [94] in DM ER experiments. Without a loss of generality, we demonstrate our results by choosing a few benchmark substructures. We expect broadly similar results for other relevant substructures. In addition, our formalism will be useful for future analysis of DM ER experiments for xenon-based targets. Currently we do not understand how much of these substructures contributes to the local DM density. We have chosen a few benchmark values of DM substructure contributions to the local DM density, namely 100%, 20%, and 10% and presented our results. Our choices are motivated by ref. [96] which states that stellar substructures near the Sun may constitute $\gtrsim 20\%$ of the stellar halo. We also consider the forecast of xenon targets in resolving the fraction of DM substructures components for a few benchmark choices of the DM parameter space.

The rest of the paper is organized as follows. In section 2, we briefly review the DM-electron scattering in xenon-based detectors. In section 3, we describe DM substructures that we have considered in our analysis. In section 4, we present our results along with the statistical methodology, and conclude in section 5.

2   DM-electron scattering at xenon

If the ambient DM particle scatters off an electron of xenon, DM may transfer its kinetic energy to the electrons, leading to free electrons. For example, a non-relativistically moving ambient DM of mass $\sim 100\,\mathrm{MeV}$ will have kinetic energy $\sim 50\,\mathrm{eV}$ (in the Solar system), which is in the ballpark of the electron ionization energy of xenon.

In a two-phase xenon time projection chamber, DM particles interact with the liquid Xe target material, and depending on interaction type (electronic or nuclear), the signal topologies are different. For DM-nuclear interaction, the deposited DM energy produces excited atoms, electron-ion pairs, and some non-observable heat. Some free electrons recombine with ionized atoms to generate more excited atoms. Essentially both the direct and excited states produced by electron-ion recombination make a characteristic scintillation light. This prompt scintillation light, known as S1, is detected in photomultiplier tubes (PMTs) immersed in the liquid Xe at the bottom. Due to an external electric field, the remaining electrons drift through liquid xenon and cross the liquid and gaseous interface,

producing proportional scintillation in the upper PMTs. This signal is known as S2. For the ER interactions, almost all the ionized electrons are collected at the upper PMTs through scintillation, producing a dominant S2 signal with a subdominant S1 signal. Hence ER interactions manifest through a large S2/S1 ratio compared to the NR case [162].

Let us consider a DM particle of mass m_χ and velocity v scattering off an electron in the xenon atom. Energy conservation implies [60]

$$v_{\min} = \frac{q}{2m_\chi} + \frac{\Delta E_e}{q}, \tag{2.1}$$

where $v_{\min}$ is the minimum DM velocity required to get an ER of ΔE_e, and q is the momentum transfer to the electron. Note that ΔE_e must be greater than the ionization energy of the corresponding shell $E_{n,l}$ to have an observable recoil E_e, i.e., $\Delta E_e = E_{n,l} + E_e$. The differential DM-electron scattering event rate can be written as [57]

$$\frac{dR}{d\ln E_e} = N_T \frac{\rho_\chi}{m_\chi} \sum_{nl} \frac{\bar{\sigma}_e}{8\mu_{\chi e}^2} \int q\,dq\, F_{\rm DM}(q)^2 \, |f_{\rm ion}^{n,l}(k',q)|^2 \, \eta\left(v_{\min}(k',q),t\right), \tag{2.2}$$

where N_T is the number of electrons in the target, ρ_χ denotes the local DM density, and DM-electron reduced mass is represented by $\mu_{\chi e}$. DM-electron scattering cross section for a reference momentum transfer, namely $q = \alpha m_e$, is indicated by $\bar{\sigma}_e$. The DM form factor, $F_{\rm DM}(q)$, takes care of the momentum dependency in the cross-section. The ionization form factor is represented by $f_{\rm ion}^{n,l}$ with n and l being the principal and angular momentum quantum number, respectively. The recoil momentum is denoted by $k' = \sqrt{2m_e E_e}$. The time dependency of the recoil signal is described through t. The quantity η, also called the mean inverse speed, depends on the $i^{\rm th}$ DM velocity distribution as

$$\eta^i(v_{\min},t) = \int_{v_{\min}}^\infty \frac{f_{\rm lab}^i(\mathbf{v},t)}{v} d^3v, \tag{2.3}$$

where $f_{\rm lab}^i$ is the DM velocity distribution at the detector's rest frame in the location of the Earth for the $i^{\rm th}$ DM component (which contributes to the DM velocity distribution). The latter can be obtained by boosting the galactic rest frame DM velocity distribution ($f_{\rm gal}$)

$$f_{\rm lab}^i(\mathbf{v},t) = f_{\rm gal}^i(\mathbf{v} + \mathbf{v}_{\rm E}(t)), \tag{2.4}$$

where $\mathbf{v}_{\rm E}$ is the Earth's velocity in the galactic rest frame:

$$\mathbf{v}_{\rm E}(t) = \mathbf{v}_{\rm LSR} + \mathbf{v}_{\rm pec} + \mathbf{u}_{\rm E}(t). \tag{2.5}$$

Here $\mathbf{v}_{\rm LSR}$ is the velocity of the local standard of rest (LSR), $\mathbf{v}_{\rm pec}$ is the peculiar velocity of the Sun with respect to the LSR. Conventionally these are expressed in galactic rectangular co-ordinate and expressed as $\mathbf{v}_{\rm LSR} = (0, v_0, 0)$, $\mathbf{v}_{\rm pec} = (11.1\pm1.5, 12.2\pm2, 7.3\pm1)$ km/s [163]. Following refs. [75, 156], throughout the paper we fix $v_0 = 233$ km/s. The uncertainties associated with v_0 and other astrophysical parameters have been studied in refs. [72, 74, 75] in the context of ER (see ref. [164] for halo independent analysis). The time-dependent Earth's velocity is represented by $\mathbf{u}_{\rm E}(t)$ which leads to the well-known annual modulation of the signal. The expression for $\mathbf{u}_{\rm E}(t)$ can be found in [165].

The differential event rate given in eq. (2.2) can be divided into three parts. The particle physics input is indicated by $\bar{\sigma}_e$ and $F_{\rm DM}$. Throughout our analysis, we will do a model-independent analysis with two choices of $F_{\rm DM}$: 1 and $1/q^2$, which appears in large classes of particle physics model [166–173]. We will present the results of $F_{\rm DM} = 1$ in the main text and that of $F_{\rm DM} = 1/q^2$ in the appendix. The atomic physics part symbolized by $f_{\rm ion}^{\rm n,l}$ signify ionization probability. The numerical values of the $f_{\rm ion}^{n,l}$ is adopted from QEdark [55, 57, 174]. The local DM density and η constitute the astrophysical inputs.

The galactic DM velocity distribution is traditionally assumed to be a Maxwell-Boltzmann (MB) distribution truncated at the galactic escape velocity ($v_{\rm esc}$)

$$f_{\rm gal}^{\rm MB}(\mathbf{v}) = \frac{1}{(2\pi\sigma_v^2)^{3/2}N_{\rm esc}^{\rm MB}} \exp\left(-\frac{|\mathbf{v}|^2}{2\sigma_v^2}\right)\Theta(v_{\rm esc} - |\mathbf{v}|). \tag{2.6}$$

The isotropic velocity dispersion σ_v is related to v_0: $v_0 = \sqrt{2}\sigma_v$. The normalization constant $N_{\rm esc}^{\rm MB} = {\rm erf}(z) - 2\pi^{-1/2}ze^{-z^2}$ with $z = v_{\rm esc}/v_0$ and erf is the error function. Throughout the discussion the galactic escape velocity ($v_{\rm esc}$) has been fixed to $528\,{\rm km/s}$ [156, 175]. While the MB distribution may describe the DM velocity distribution which is in equilibrium (hydrodynamical simulations indicate that MB distributions may not adequately describe the velocity distribution of the smooth DM halo component), the equilibration condition will not be met for relatively recent mergers of the MW with other galaxies. These recent mergers will have unique signatures, both in velocity and position space, called substructures. The existence of these substructures is also observed in various N-body simulations. When a galaxy accretes into the Milky Way, the stellar component of the accreted galaxy carries several tell-tale signatures: stellar streams, stellar shards, and stellar debris flow [85–97].

The recent results of various surveys like Gaia, SDSS, and LAMOST indeed indicate the presence of these stellar substructures. Combining the effect of the substructure with the SHM, we get total average inverse speed as

$$\eta(v_{\rm min}, t) = \int_{v_{\rm min}}^{\infty} \frac{1}{v} \left[(1 - \delta)f_{\rm lab}^{\rm MB}(\mathbf{v}, t) + \delta f_{\rm lab}^{\zeta_i}(\mathbf{v}, t)\right] d^3v, \tag{2.7}$$

where $f_{\rm lab}^{\zeta_i}(\mathbf{v}, t)$ refers to the substructure velocity distribution (discussed in section 3) and δ represents the fractional contribution that the corresponding component constitutes to the local density of DM.[2] In what follows, we will consider the effect of these substructures in DM velocity distribution and the ER DD rate in liquid xenon experiments.

3 DM substructures

This section discusses the benchmark DM substructures that we have studied in this work. We have utilized the results of ref. [94] where the stellar substructure is obtained using the star catalog of LAMOST DR3 [101]. We choose a few representative substructures to present our results. For clarity, we also mention the name of the associated dynamically tagged

---

[2]If each of the substructures contributes different fractions then instead of one δ there will be a set of such δ's. For simplicity, we have ignored the effect of multiple substructures.

Substructure	Mean velocity (km/s)			Velocity dispersion (km/s)		
	μ_R	μ_ϕ	μ_z	σ_R	σ_ϕ	σ_z
HelmiDTG1	4.5	197.2	244.3	146.0	62.6	42.4
HelmiDTG3	26.2	157.1	-241.3	78.9	28.8	27.2
PolarDTG11	-47.9	21.8	229.2	75.4	19.2	21.5
PgDTG2	221.2	155.7	139.7	26.2	33.8	52.3
Sausage	2.1	-0.3	-8.7	136.6	35.0	72.3
RgDTG28	-4.0	-106.1	-143.2	115.8	29.3	30.3
Sequoia	-36.9	-273.9	-87.0	138.2	36.7	65.0

Table 1. The details of the substructures are used in this paper. The numerical values of the mean velocities and diagonal values of the velocity dispersions are adapted from tables 2 and 3 of [94]. The DTG from which substructures are identified has also been specified.

groups (DTG) with the relevant substructures [94]. The details of these substructures are summarised in table 1. We emphasize that the chosen substructures are for illustrative purposes only. Further research is required in order to understand the DM content of various substructures and whether the substructure DM profile coincides with the Solar circle. Whether the corresponding DM substructure will follow the same velocity distribution as the stellar substructure or not is currently not understood. Using Via Lactea II high-resolution N-body simulation, it has been shown that DM debris flows closely follows their stellar counterpart [89, 113]. However, the same is not valid for Sagittarius stream [112]. Nevertheless, we will assume that the velocity distributions of the substructures follow that of the corresponding stellar components. This assumption can be confirmed or refuted by future research. However, the broad conclusion (like the change in the event rate and subsequently in the discovery limit due to DM substructures) of this study will hold.

We note that the substructures we have considered in this paper have similarities with previous considerations [73, 114]. For instance, the Helmi substructure is analogous to S2-substructure [109]. The velocity properties of the Nyx substructure are somewhat similar to the prograde (Pg) stream and are expected to arise from the same Splashed Disk event [94].[3] Some of the considered substructures are also found in Gaia DR3 data at the Solar neighborhood [95, 96, 161].

The mean stellar velocities and the diagonal values of the stellar velocity dispersions are given in table 1. In general, DM substructures will have a different velocity distribution than the virialized component (SHM), which will dramatically impact the ER distribution. The galactic velocity distribution for each of the substructures (referred to by ζ_i) can be written as [73, 114]

$$f_{\text{gal}}^{\zeta_i}(\mathbf{v}) = \frac{1}{(8\pi^3 \det \sigma^{\zeta_i})^{1/2} N_{\text{esc}}^{\zeta_i}} \exp\left(-(\mathbf{v} - \boldsymbol{\mu}^{\zeta_i})^T \frac{1}{2(\sigma^{\zeta_i})^2}(\mathbf{v} - \boldsymbol{\mu}^{\zeta_i})\right) \Theta(v_{\text{esc}} - |\mathbf{v}|), \quad (3.1)$$

where σ^{ζ_i} is the velocity dispersion matrix, assumed to be diagonal with the values given in table 1 and $\det \sigma^{\zeta_i}$ is the determinant of the dispersion matrix. The mean velocities of

---

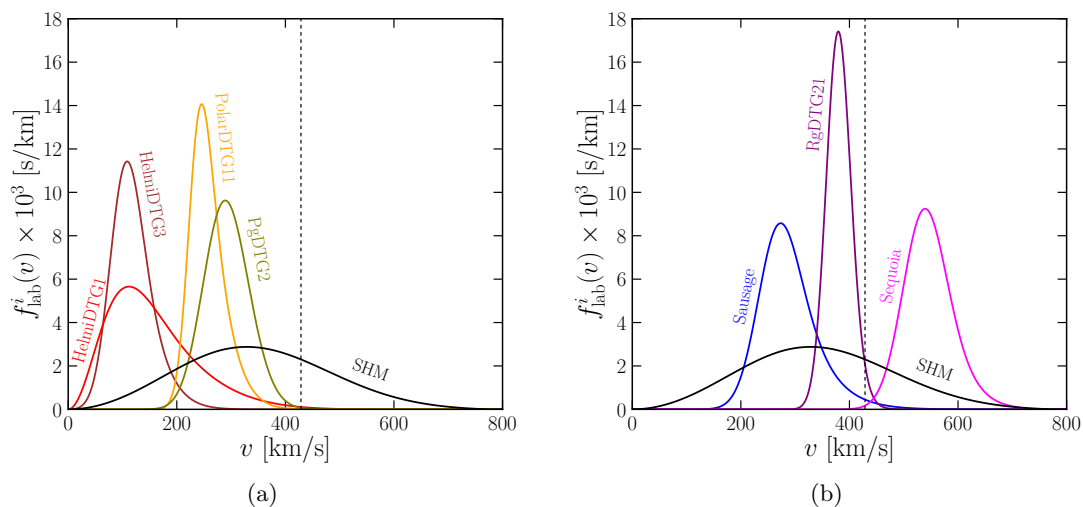[3]Ref. [176] has argued that Nyx is a part of thick disk.

Figure 1. We show the lab frame DM speed distributions for all the considered astrophysical components. The red, brown, orange, olive, blue, purple, and pink solid lines represent the HelmiDTG1, HelmiDTG3, PolarDTG11, PgDTG2, Sausage, RgDTG28, and Sequoia, respectively. We also display the same for SHM by the solid black line. The vertical dashed line shows required $v_{\min}$ for $m_\chi = 100\,\mathrm{MeV}$ with $E_e = 20\,\mathrm{eV}$, $q = 25\,\mathrm{keV}$, and $5p^6$ shell.

the substructures in the galactic frame are expressed by $\boldsymbol{\mu}^{\zeta_i}$ which are non-zero in contrast to the SHM case, as indicated in table 1. The normalization constant $N_{\mathrm{esc}}^{\zeta_i}$ is calculated numerically. The step function represents the cut-off at the galactic escape velocity, although the substructures' velocity distributions are likely to peak at smaller velocities. Therefore this cut-off will have a numerically insignificant effect. The index ζ_i refers only to the substructure, whereas i includes both the substructures and SHM.

Assuming eq. (3.1) as the galactic velocity distributions for the DM substructures, we display the corresponding lab frame speed distributions, $f_{\mathrm{lab}}^i(v) = v^2 \int d\Omega f_{\mathrm{lab}}^i(\mathbf{v})$, using eq. (2.4) in figure 1. Except for the modulation signature (discussed in section 4.3), we fix the Earth's velocity to $\mathbf{v_E} = (39.7, 243.2, 16.4)\,\mathrm{km/s}$ to economize the computation. This value of $\mathbf{v_E}$ is attained during first week of March when the Earth's velocity is roughly equal to its average velocity. For Sequoia we have explicitly checked that taking the exact yearly average rate would lead to less than $\sim 6\%$ change in the discovery limit. Given the poor knowledge of DM substructure fraction, we ignored this $\lesssim 10\%$ effect. The general trend we observe is that the substructures which peak at larger values of v have negative μ_ϕ. Since the Earth moves with high positive rotational velocity ~ 250 km/s, substructures with negative μ_ϕ, will hit the Solar system with larger velocities. On the other hand, substructures having large positive μ_ϕ co-rotate with the Earth, leading to $f_{\mathrm{lab}}^i(v)$ peaking at smaller velocities. This has been displayed in figure 1, where the Helmi streams having larger values of μ_ϕ peak at relatively smaller velocities, whereas Sequoia having a negative μ_ϕ peaks at the higher velocity. We also display the velocity distribution of SHM by the solid black line. For reference we show the required $v_{\min} = 428.7$ km/s to obtain a recoil of $20\,\mathrm{eV}$ with momentum transfer $25\,\mathrm{keV}$ and $5p^6$ shell for DM mass $100\,\mathrm{MeV}$ by the vertical black dashed line.
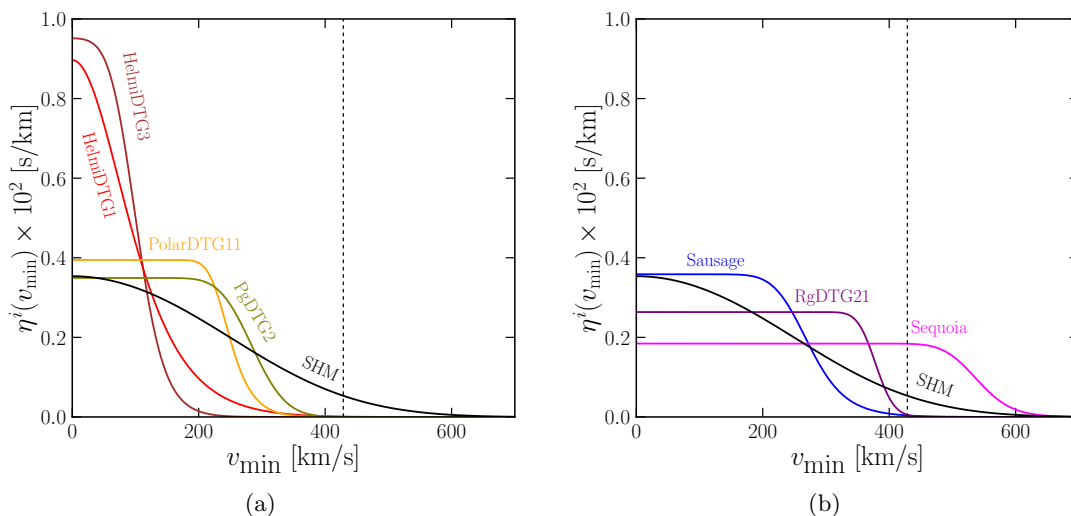
Figure 2. The mean inverse speed ($\eta^i(v_{\min})$) for the considered substructures and the SHM. The color coding and other relevant details are same as figure 1.

Given these velocity distributions, we turn to the discussion of the mean inverse speed $\eta^i(v_{\min})$ (using eq. (2.3)) of each of the astrophysical components. The values of $\eta^i(v_{\min})$ as a function of $v_{\min}$ are depicted in figure 2. The vertical black dashed line indicates values of $\eta^i(v_{\min})$ for $v_{\min} = 428.7$ km/s. Expectedly, $\eta^i(v_{\min})$ are monotonically decreasing function of $v_{\min}$, which can be understood from the integration over velocity starting from $v_{\min}$. The maximum values of $\eta^i(v_{\min})$, i.e., $\eta^i(0)$ is larger for the distributions which peak at lower velocities because the mean inverse speed is inversely proportional to the most probable speed (the speed at which velocity distribution attains maximum value) of the distribution. Hence in figure 2, we observe maximum and minimum $\eta^i(0)$ for HelmiDTG3 and Sequoia respectively. For the other distributions, $\eta^i(0)$ lie within the same of HelmiDTG3 and Sequoia. The flatness of $\eta^i(v_{\min})$ for Sequoia up to a large value of $v_{\min}$ as compared to other distributions is also a manifestation of the higher most probable speed of Sequoia. This indicates the extent to which $v_{\min}$ is supported by the distribution. It should also be noted that the flatness of $\eta^i(v_{\min})$ is also sensitive to the choice of the velocity dispersion.

4 DM-electron scattering at xenon: effect of substructure

In this section, we discuss the effect of the substructures on the DM-electron scattering rate for liquid xenon experiments. For $F_{\rm DM}(q) = 1$, the constraint on the DM-electron scattering cross-section from the xenon detectors dominate when DM mass is $\gtrsim 50$ MeV. Xenon experiments may have a better prospect of discovering DM-electron scattering, and it is essential that we study this prospect thoroughly. Our work outlines the theory effort toward answering this important question.

Following ref. [57], we convert the ER energy (E_e) to number of electrons (n_e). DM-electron scattering would produce n_e number of observable electrons, unobservable photons, and heat. Some primary electrons would recombine with secondary ions with probability
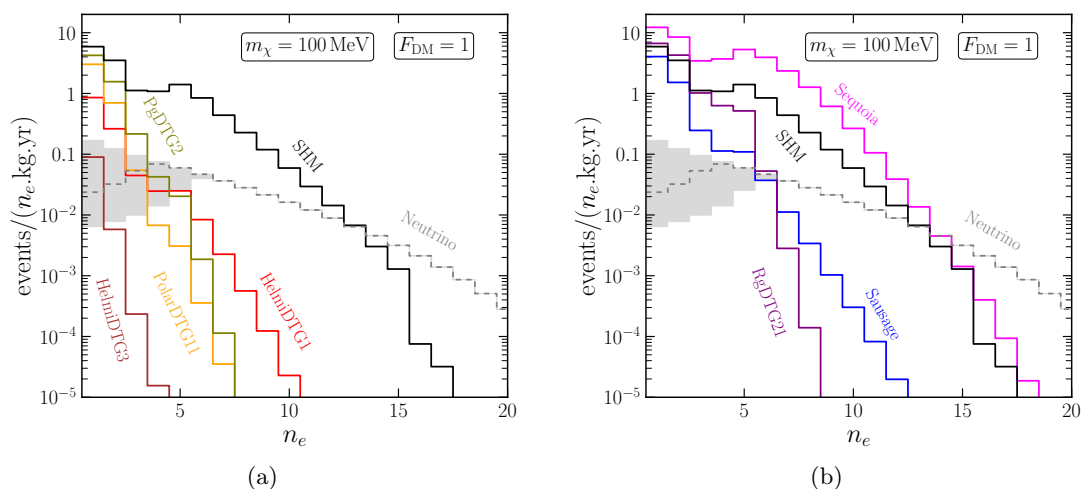
Figure 3. Differential event rate as a function of number of electron n_e with exposure of 1 kg-year, for $m_\chi = 100\,\text{MeV}$, and $\bar{\sigma}_e = 10^{-40}\,\text{cm}^2$ assuming each of the labelled astrophysical component contribute 100% to the local DM density. The neutrino-induced event rates are illustrated by the grey dashed lines, and the grey shaded regions represent the variation in the event rates for different ionization models.

f_R. Further, each recoiling electron of energy E_e will give rise to additional secondary $n_e^{(1)} = \text{Floor}[E_e/W]$ quanta (photon or electron). The average energy required to create a single quanta is W. Moreover, the scattering process can also lead to the ionization of electrons from the inner shell, which would de-excite by releasing a photon. These photons may also create secondary quanta, $n_e^{(2)} = \text{Floor}[\Delta E_{i,j}/W]$, $\Delta E_{i,j}$ is the difference between binding energies between the relevant inner and outer shells. The number of secondary electrons produced is calculated using a binomial distribution with $n_e^{(1)} + n_e^{(2)}$ trials, having success probability f_e. We have chosen fiducial values (i.e., $W = 13.6\,\text{eV}$, $f_e = 0.83$, $f_R = 0$) of the relevant parameters to convolute eq. (2.2) which will give the differential event rate as a function of number of produced electrons. Our paper does not consider uncertainties associated with W, f_e, and f_R.

In figure 3, we show the differential event rate as a function of n_e for $m_\chi = 100\,\text{MeV}$, $\bar{\sigma}_e = 10^{-40}\,\text{cm}^2$, and 1 kg-year exposure. For each event rate, we have assumed that the corresponding astrophysical component (SHM or substructures) constitutes 100% of the local DM density. For $m_\chi = 100\,\text{MeV}$ with typical momentum transfer of $\mathcal{O}(10)\,\text{keV}$, to obtain a measurable recoil the required minimum DM velocity should be around $500\,\text{km/s}$. Hence, the tail of $\eta^i(v_{\min})$ dominantly contributes to the recoil rate. Evidently the substructures having the largest value of $\eta^i(v_{\min})$ near $v_{\min} \sim 500\,\text{km/s}$ give rise to a larger event rate.

4.1 Neutrino background

The scattering of neutrinos with electron/ nucleon may also give rise to ionization signals in low-threshold DD experiments. Other background sources like radioactive background, Cherenkov radiation, etc. which can potentially mimic a DM signal [177]. The experimental

collaborations confront and beat these non-neutrino backgrounds using various experimental techniques to isolate a potential DM signal. However, the neutrinos are an irreducible background that can not be removed by using shielding, purified detector material, and other experimental techniques. Because of this, we have taken neutrinos as the only source of background in our analysis. If other non-neutrino backgrounds are found in the data-set, then our results will degrade proportionally.

It has been argued in refs. [178, 179] that Solar neutrinos are the main source of background for sub-GeV DM-electron scattering.[4] Neutrino-electron elastic scattering is the dominant contribution of background events for rather large recoil energy ($\sim 10^5$ eV). Instead, coherent neutrino-nucleon scattering may produce small ionization, which would be the dominant source of background in our consideration. The neutrino-nucleon scattering event rate is [178, 181]

$$\frac{dR}{dE_{\mathrm{NR}}} = N_T M T \int_{E_\nu^{\mathrm{min}}} \frac{d\sigma}{dE_{\mathrm{NR}}} \frac{d\phi_\nu}{dE_\nu} dE_\nu, \tag{4.1}$$

where N_T, M, and T are the number of target nuclei per unit mass, total mass, and time respectively. The minimum neutrino energy to produce a nuclear recoil of energy E_{NR} is expressed by $E_\nu^{\mathrm{min}} = \sqrt{m_N E_R/2}$. The differential coherent neutrino nucleon cross section and the differential neutrino flux are denoted by $d\sigma/dE_{\mathrm{NR}}$ and $d\phi_\nu/dE_\nu$ respectively [178, 182]. We have utilized low, fiducial, and high ionization models given in ref. [178] to obtain number of electron n_e for a particular nuclear recoil energy. The corresponding neutrino-induced event rate for fiducial model is displayed in figure 3 by the grey dashed lines.[5] The grey shaded regions represent variation in the event rate for high and low ionization models of n_e [178]. Since there is a difference between three ionization models in the low n_e/energy bins, hence we observe a large change in the differential event rates at those bins. The discovery limits for low and high ionization models is given in appendix C. For one electron threshold, the impact of the ionization model uncertainty leads to less than a factor of 3 change in the discovery limits.

4.2 Statistical methodology

In this section, we discuss the statistical procedure to obtain the discovery limit for DM-electron scattering in the presence of substructures for liquid xenon experiments. We have employed the profile likelihood ratio test [183] with $\bar{\sigma}_e$ and substructure fraction (δ) as the signal parameters of interest. In the following, we briefly discuss this procedure.

The binned likelihood for the background and signal model ($\mathcal{M}$), is given by

$$\mathcal{L}(\mathcal{D}(\theta)|\mathcal{M}(\theta)) = \prod_{i=1}^{n_{\mathrm{bins}}} \left(\mathcal{P}(N_{\mathrm{obs}}^i | N_\chi^i + \sum_{j=1}^{n_\nu} n_\nu^i(\Phi^j)) \right) \prod_{j=1}^{n_\nu} \mathcal{G}(\Phi^j) \tag{4.2}$$

Here $\theta = (m_\chi, \bar{\sigma}_e, \delta, \Phi)$ and $\mathcal{D}(\theta)$ is the Asimov data set. The number of energy bin is represented by n_{bins}. The Poisson probability ($\mathcal{P}$) at the i-th bin is calculated using observed

---

[4]See refs. [178, 180] or discussion related to the prospect of these detectors in probing beyond SM interactions of neutrino.

[5]We note that there is a factor ~ 3 difference in the event rate between our result and ref. [178].

N^i_{obs} and the expected number of events. The expected number of events is the addition of DM events (N^i_χ) and the sum of neutrino events (n^i_ν) for all the neutrino components (n_ν). The Gaussian function $(\mathcal{G}(\Phi^j))$ takes care of the uncertainty in the neutrino fluxes (Φ^j) with mean values and standard deviation given in [178, 182].

Depending on the choice of the analysis, we vary one of the signal parameters (either $\bar{\sigma}_e$ or δ), treating the other one as a nuisance parameter. We treat $\bar{\sigma}_e$ as the signal parameter for the discovery reach. Therefore, the profile likelihood ratio test statistic, which compares the background-only hypothesis $(\mathcal{M}_0)$ with the background and signal model $(\mathcal{M})$, is given by [73, 183, 184]

$$q_0 = -2\ln\left(\frac{\mathcal{L}(\bar{\sigma}_e = 0, \boldsymbol{\lambda}|\mathcal{M}_0)}{\mathcal{L}(\bar{\sigma}_e, \boldsymbol{\lambda}|\mathcal{M})}\right) \sim \chi_1^2, \tag{4.3}$$

where $\boldsymbol{\lambda}$ contains the nuisance parameters, i.e., δ and Φ^j in this case. Using Wilks' theorem, it can be shown that the ratio in eq. (4.3) follows a χ^2 distribution with one degree of freedom [73, 183]. Thus, the significance of rejecting the background-only hypothesis is given by $\sqrt{q_0}$-σ. In this paper, we present all the discovery limits at the 90% confidence level (CL). We obtain the discovery limits utilizing Asimov data set which assumes that the number of observed events is same as the expected events. However in a real experimental data-set, this will not be true and in that case one should treat experimental data as the observed events. Then it would be possible to constrain $\bar{\sigma}_e$ assuming a value of substructure fraction.

We consider δ as the signal parameter for the prospective detection of DM substructure fraction. The corresponding profile likelihood ratio test to distinguish two neighboring points δ_1 and δ_2 can be written as [73]

$$q_0 = -2\ln\left(\frac{\mathcal{L}(\delta_2, \boldsymbol{\lambda}|\mathcal{M}_{\delta_1})}{\mathcal{L}(\delta_2, \boldsymbol{\lambda}|\mathcal{M}_{\delta_2})}\right) \sim \chi_1^2. \tag{4.4}$$

This profile likelihood ratio is employed to reject the null hypothesis, which is that two neighboring points δ_1 and δ_2 are indistinguishable at 68% CL. Both for eqs. (4.3) and (4.4) we utilized Asimov data set [183] to obtain the likelihood ratio test. In this scenario, artificial data is generated using the model's parameters (in our case $\mathcal{M}$). Then the expectation is that the number of observed events (N_{obs}) should be equal to the number of the expected event (N_{exp}). For a sufficiently large number of observations, the value of the profile likelihood ratio test approaches the median value. Compared to the Monte Carlo simulation, the Asimov data set scenario is computationally more economical while acquiring accurate results. For the 68% and 90% CL limit the required q_0's are 0.99 and 2.71 respectively. For a fixed m_χ and δ, the 90% CL discovery limit is obtained by changing $\bar{\sigma}_e$ in eq. (4.3) until the required q_0 (2.71) is achieved. The 68% CL contours in resolving substructure fraction are estimated using eq. (4.4). In this case for a fixed values of m_χ, σ_e, and δ_1, we iterate over δ_2 until the required q_0 ($= 0.99$) is attained.

4.3 Results

Here we will present the results using the statistical analysis discussed in the previous subsection. The three parameters of interest are DM mass (m_χ), DM-electron cross section $(\bar{\sigma}_e)$, and the DM substructure fraction (δ). Given that DM has to be massive, we present our results through two possible choices, keeping one of the other two parameters to a
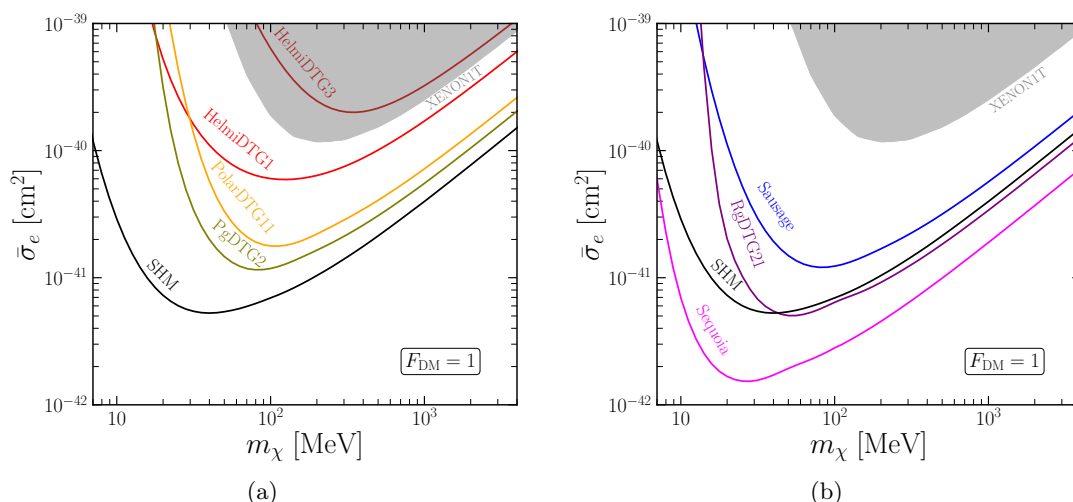
Figure 4. Discovery limits at the 90% CL for different DM substructures considered in this paper, assuming that each astrophysical component accounts for 100% of the local DM density. The discovery limits are obtained using one kg-year exposure, one electron threshold, and $F_{\rm DM} = 1$.

fixed value. In the first part, the results are presented through the discovery limit, which is depicted in DM mass and DM-electron cross-section plane keeping a fixed DM substructure fraction. In the other case, considering a fixed DM-electron cross-section, we present the forecast of the xenon experiments to resolve the substructure fraction for a few benchmark choices of DM particle masses.

In figure 4, we present the sensitivity to DM-electron cross-sections for each of the substructures considered in this paper, assuming that the corresponding substructure constitutes 100% of the local DM density. In figure 4, each line represents the minimum DM-electron cross section required to observe the effect of the corresponding substructure in a liquid xenon detector with 1 kg-year exposure and one electron threshold. The discovery limits for two and three electron thresholds are given in appendix B. The different discovery limits for different substructures are the implication of non-identical most probable speed. The tail of the DM velocity distribution will be more populous for the substructure having a relatively larger most probable speed. Therefore a sizable number of DM particles will be available to interact with the target electrons. This leads to a larger event rate, as has been depicted in figure 3, where for a fixed DM-electron cross section among the considered DM substructures, we obtain the minimum and the maximum number of events for HelmiDTG3 (lowest most probable speed, see figure 1a) and Sequoia (highest most probable speed, see figure 1b) respectively. Owing to this, the DM-electron cross-section that can be probed for HelmiDTG3 is the largest, whereas the same for Sequoia is the lowest. The event rates and subsequently the discovery limits lie between HelmiDTG3 and Sequoia for the other considered substructures. The light grey shaded region demonstrates the constraint from the ionization signals in the XENON1T experiment [63], which is the most stringent current DD constraint for the parameter space shown in the plot. For reference, we have also shown the discovery limit for the SHM with the solid black line.
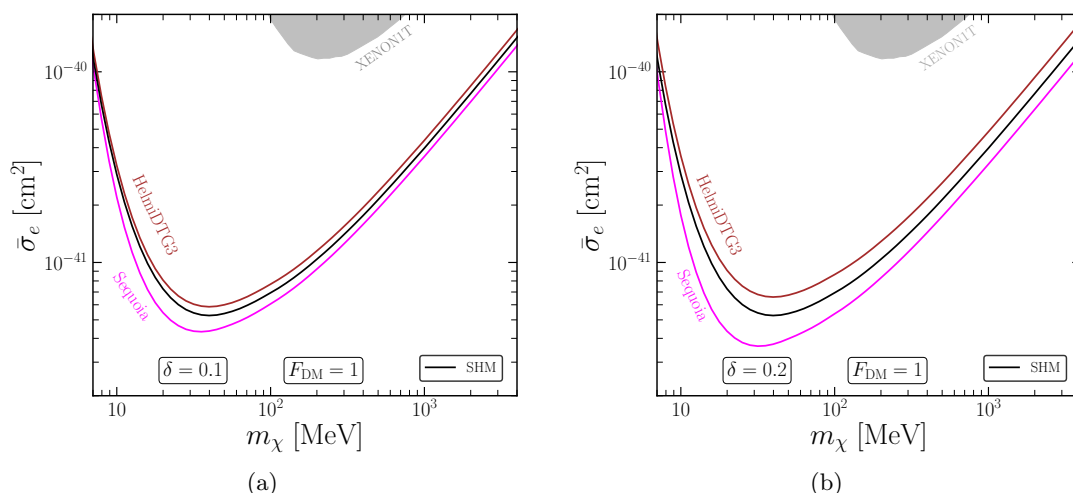
Figure 5. Discovery reach of the DM-electron cross-section at the 90% CL with combined velocity distributions. SHM combined with HelmiDTG3 and Sequoia are shown by the brown and pink solid lines, respectively. The solid black line demonstrates the pure SHM. The discovery limit presented here is for one kg-year exposure, $F_{DM} = 1$, and one electron threshold. In the left and right panel we show the results for $\delta = 0.1$ and $\delta = 0.2$, respectively.

In reality, these substructures may not contribute 100% to the local DM density. Therefore, we choose two benchmark values of δ, namely $\delta = 0.1$ and $\delta = 0.2$ (shown in figure 5). Further, as mentioned above, we have only considered two substructures, HelmiDTG3 and Sequoia, which lie at two extreme ends. SHM constitutes the rest of the local DM density for the combined DM distribution. If the discovery limit for a particular substructure (with $\delta = 1$) is larger compared to SHM, then the same for the combined DM distribution will lie above the SHM limit. This effect would be more pronounced upon increasing δ. In figure 5, the combined discovery limit for HelmiDTG3 and Sequoia is displayed by brown and purple lines, respectively. Notably, brown and purple lines lie above and below the SHM scenario. Upon increasing the δ, we observe more deviation from SHM. Importantly, it is still possible to see the effect of these substructures in liquid xenon experiments with this kind of realistic choice of δ. Next, we turn into the discussion of resolving substructure fractions in liquid xenon experiments. Again, we have restricted ourselves to HelmiDTG3 and Sequoia among the considered substructures as these two reside in the extreme ends. The sensitivity in resolving DM substructure at 68% CL is displayed in figure 6 for 1 kg-year exposure, one electron threshold, and $\bar{\sigma}_e = 10^{-40}\,\mathrm{cm}^2$, with a few benchmark points. Generically, we observe a better resolution for low DM mass. Comparing figures 6a and 6b one can see that we will determine the substructure fraction more accurately for Sequoia compared to HelmiDTG3. This is due to Sequoia's large most probable velocity, which leads to a substantial number of DM-electron scattering events. Generically, it is possible to measure the substructure fraction more accurately, which is moving with a higher most probable speed. For $\delta = 0.1$, with the considered exposure, threshold, and $\bar{\sigma}_e$, it is difficult to conclude whether the substructure is contributing to
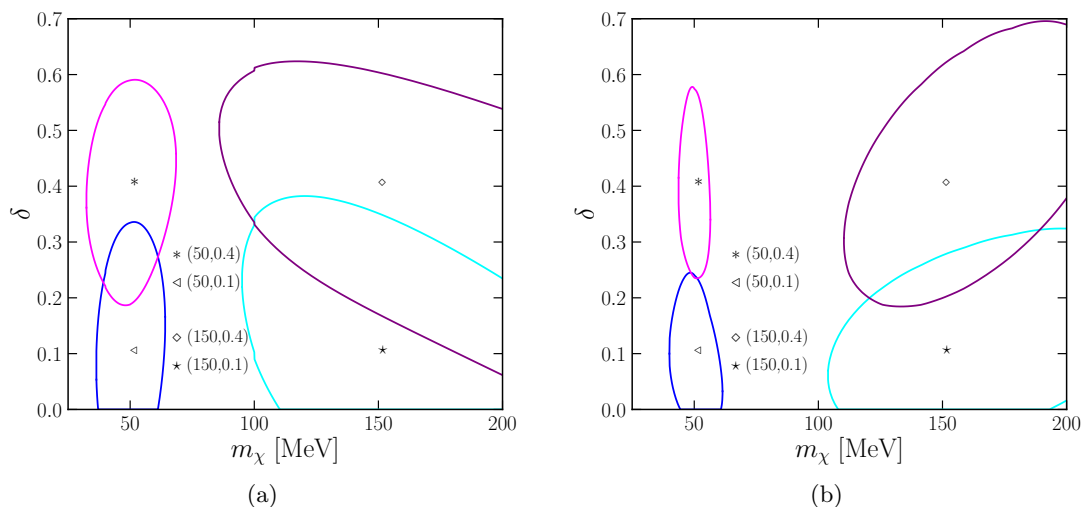
Figure 6. 68% CL contours in $m_\chi - \delta$ plane, representing forecast in resolving DM substructure fraction for a few benchmark points. We have assumed 1 kg-year exposure, one electron threshold, $\bar{\sigma}_e = 10^{-40}\text{cm}^2$, and $F_{\text{DM}} = 1$. In the left and right panels, we show the results for HelmiDTG3 and Sequoia, respectively.

local DM density. Interestingly, for DM mass $\sim 50\,\text{MeV}$, and $\delta = 0.4$, xenon target electron scattering experiments can resolve the substructure fraction with $\sim 50\%$ accuracy. Moreover, the structures of the contours can be understood from eq. (2.1) and from figure 2. Both for the lower and higher DM masses, the inclination of the contours is reversed as we compare HelmiDTG3 with Sequoia. For low DM masses, v_{min} is larger (for fixed q and E_e from eq. (2.1)), therefore it is the tail of the distribution which is contributing to η^i. Thus for HelmiDTG3 with low mass DM, an increment in δ will reduce the combined value of η. This reduction could be compensated by increasing DM mass for a fixed number of observed events. This results in a slightly tilted contour towards a higher DM mass. Whereas for higher DM mass (thus smaller v_{min}), the maximum value of η determines the orientation of contours. For Sequoia, the maximum value of η^i is less than that of HelmiDTG3. Hence increasing δ for the former will reduce combined η, which can be elevated by reducing v_{min}, i.e., by increasing DM mass.

We have not discussed a distinctive feature of the DM DD signal: annual modulation [54], where the signal event rates vary with the time of the year in a specified manner. Due to the rotation of the Sun around the MW, there will be DM wind in the Solar rest frame. Due to the Earth's rotational motion around the Sun, the event rate will vary with time. For the SHM, the event rate will be larger (smaller) when the Sun and the Earth travel in opposite (same) directions, respectively. Due to this distinctive feature, which the background cannot mimic, annual modulation events are expected to be less dependent on the background reductions and identifications.

Unlike non-modulation case here we take into account variation of $\mathbf{v_E}$ over time. The main task for the modulation discovery limit would be to evaluate the event rate against both time and energy (N_{tim}). For a particular energy bin, we obtain modulation events

($N_{\rm mod}$), by subtracting each time bin events from average time bin events ($N_{\rm avg}$). We do the same exercise for all the energy bins. The corresponding likelihood can be obtained by taking the difference of their individual Poisson distributions, referred to as the Skellam distribution [185]

$$\mathcal{L}(\mathcal{D}(\theta)|\mathcal{M}(\theta)) \equiv \prod_{j=1}^{n_{\rm t}} \prod_{i=1}^{n_{\rm bins}} e^{-(N_{\rm tim}(i,j)+N_{\rm avg}(i))} \left(\frac{N_{\rm tim}(i,j)}{N_{\rm avg}(i)} \right)^{N_{\rm mod}(i,j)/2}$$
$$I_{N_{\rm mod}(i,j)} \left(2\sqrt{N_{\rm mod}(i,j)N_{\rm avg}(i)} \right), \qquad (4.5)$$

where, i and j represent each time and energy bin and $n_{\rm t}$ is the total number of time bins. The modified Bessel function of the first kind is denoted by $I_{N_{\rm mod}}$. We utilized eq. (4.5) to obtain test statistics (given in eq. (4.3)) and subsequently the discovery limit. Following this prescription [73], we find that the modulation discovery limit is weaker than the non-modulation counterpart. For example, with SHM or Sequoia, we observed that the modulation discovery reaches are weaker by a factor $\sim 10 - 100$.

5 Conclusions

The presence of DM in the Universe is well established. Many attempts have been made to discover the connection between DM and SM states. Among them, DD experiments look for the scattering signatures of DM and visible states. There has been a growing interest in the search for light DM (masses $\lesssim 1\,{\rm GeV}$) through DD. Ambient non-relativistic DM having mass in the sub-GeV range can not impart sufficient energy to produce a measurable recoil in the typical nuclear recoil DD experiments. Electron, being a light particle, can be an excellent target in detecting such light DM. Many target materials have been considered to identify electronic excitation by the scattering of ambient DM. DM velocity distribution is an integral part of calculating the event rate or the exclusion limit of the DD experiments. DM is also an intrinsic part of structure formation; the history of galaxy formation influences its velocity distribution. While it is difficult to track the velocity distribution of DM, however, it may be manifested through stellar distribution. Surveys like Gaia, SDSS, LAMOST, etc., have made unprecedented progress mapping these stellar distributions. These data reveal the presence of stellar clumps and substructures. It is highly likely that there is a DM counterpart to these stellar substructures, called DM substructure. This paper investigates the prospects of detecting these substructures in low threshold DM DD experiments through elastic DM-electron scattering. Specifically, we have explored the prospect of xenon targets experiments in deciphering this. Note that compared to semiconductor targets experiments (like SENSEI), the xenon targets experiments have better sensitivity in the DM mass range of $\mathcal{O}(100)\,{\rm MeV}$.

We utilize the results of the LAMOST survey and choose a few benchmark DM substructures. We emphasize that there is no definite proof of the existence of the DM counterpart to the detected stellar substructures. However, it is likely that they exist. If these DM substructures overlap with the Earth's position, then we can observe the imprint of the same in xenon targets experiments through DM-electron scattering. We find that

if the substructure constitutes $\gtrsim 10\%$ of the local DM density, then there is a possibility to observe the effect of the substructures in xenon target experiments with the currently allowed DM particle properties. We have also explored the forecast of xenon experiments in resolving the DM substructure fraction. We find that the uncertainty in resolving DM substructure fraction is considerable for higher DM mass compared to lower DM mass. For example, with $m_\chi = 50\,\text{MeV}$, $\bar{\sigma}_e = 10^{-40}\,\text{cm}^2$, and one electron threshold in xenon experiments, we can resolve the substructure fraction to $\sim 50\%$ accuracy provided $\delta \sim 0.4$. The discovery limit and resolving DM substructure fraction are mainly regulated by the most probable velocity of the corresponding velocity distribution. Given this correlation between DD rates and DM velocity distributions, a more detailed understanding of DM substructure is required. High-resolution cosmological simulations and near-future observations will play a crucial role in understanding this. We encourage the experimentalists to continue their excellent work in improving their detector sensitivity so that we are sensitive to such a signal. Our work shows that by pursuing this technique, we will be able to know more about the particle physics and astrophysics of DM and maybe even discover it.

Acknowledgments

A Event rate

In this appendix we provide event rate for DM mass 50 MeV. This is displayed in figure 7.

B Discovery limits for two and three electron threshold

Throughout the main text, we have considered the reach of the xenon experiments for one kg-year exposure and one electron threshold with $F_{\text{DM}} = 1$. Here we present the discovery limit with two and three electron thresholds for $\delta = 0.1$. The results are depicted in figures 8a and 8b. With higher thresholds, the expected event numbers decrease; thus, the required cross-section to see the possible effect of the substructure increases. Further, the lowest possible DM mass that can be probed also increases.

C Variation in the discovery limits

As discussed in section 4.1, background event rate from neutrino may change depending on the ionization model. In this appendix, we present the discovery limit for high and low ionization efficiencies models for n_e [178]. We display the result in figure 9. For each of the substructures, solid lines represent discovery limits for fiducial ionization model and shaded bands show the corresponding uncertainties associated with the ionization models.
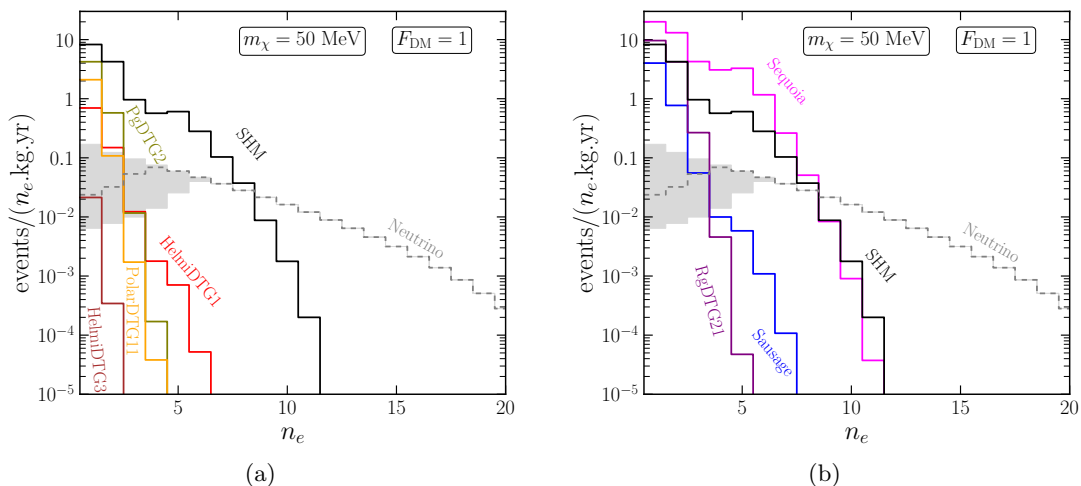
Figure 7. Differential event rate as a function of number of electron n_e for $m_\chi = 50\,\text{MeV}$. Other relevant details are same as figure 3.
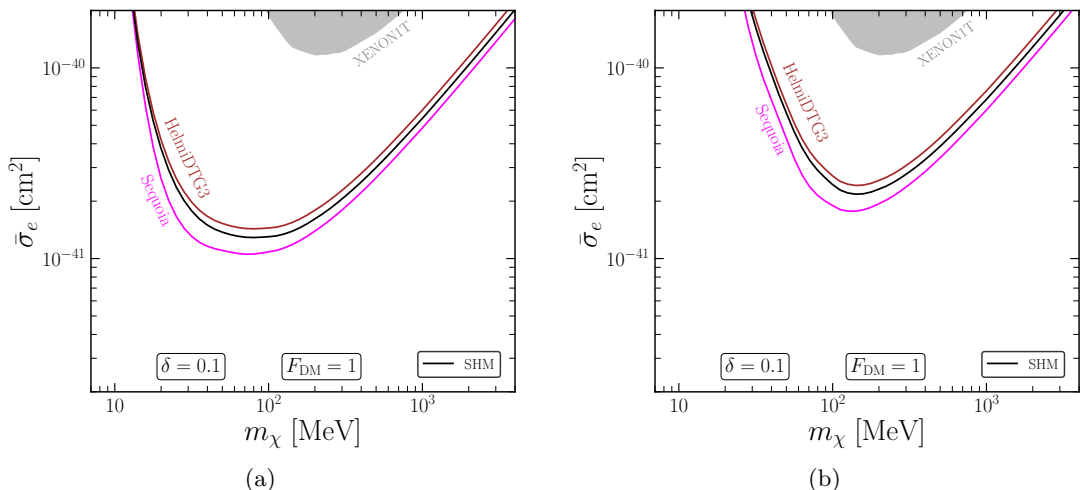

Figure 8. Discovery limits at the 90% CL for the considered DM distribution with $F_{\text{DM}} = 1$, one kg-year exposure. Each of the considered substructures contributes 10% to the DM density. (a) For two electron threshold. (b) For three electron threshold.

D Momentum dependent DM-electron scattering

In this appendix, we present the discovery limits of the momentum-dependent DM-electron scattering, namely $F_{\text{DM}} = \alpha^2 m_e^2/q^2$ for the considered DM substructures. In this case, we also observe a similar tendency, except that the minimum required DM-electron cross section for the discovery of the substructures is larger than the same of $F_{\text{DM}} = 1$. This is displayed in figure 10.
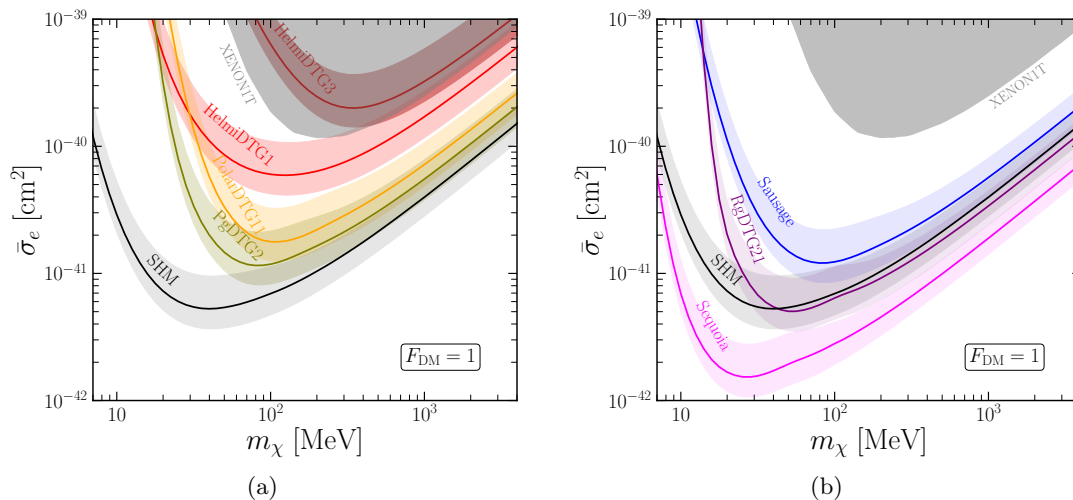
Figure 9. Variation in the discovery limits due to high and low ionization efficiency models for n_e [178] assuming one electron threshold. For each of the substructures the corresponding light shaded bands represent the uncertainties that may arise from different ionization models of n_e. Each of the substructures contribute to 100% to local DM density.
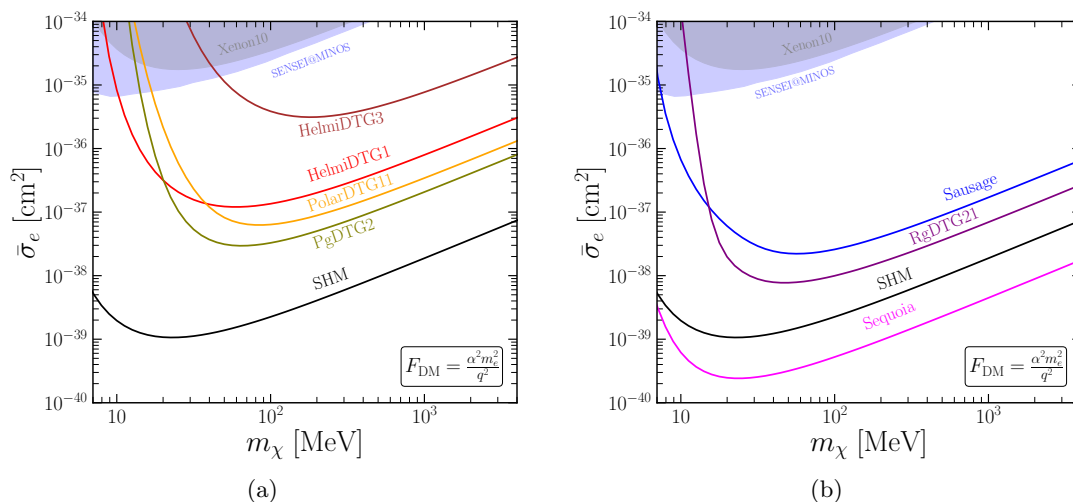

Figure 10. Discovery limits at the 90% CL for the considered DM distribution with $F_{\rm DM} = \alpha^2 m_e^2/q^2$. We have assumed one kg-year exposure and one electron threshold to obtain the discovery limit. The Xenon10 [57] and SENSEI@MINOS [70] limit has also been shown by the grey and blue shaded regions.

References

[1] G. Bertone, D. Hooper and J. Silk, *Particle dark matter: Evidence, candidates and constraints*, *[Phys. Rept.](https://doi.org/10.1016/j.physrep.2004.08.031)* **405** (2005) 279 [[hep-ph/0404175](https://arxiv.org/abs/hep-ph/0404175)] [[INSPIRE](https://inspirehep.net)].

[2] T. Lin, *Dark matter models and direct detection*, *[PoS](https://doi.org/10.22323/1.333.0009)* **333** (2019) 009 [[arXiv:1904.07915](https://arxiv.org/abs/1904.07915)] [[INSPIRE](https://inspirehep.net)].

[3] T.R. Slatyer, *Les Houches Lectures on Indirect Detection of Dark Matter*, *[SciPost Phys. Lect. Notes](https://doi.org/10.21468/SciPostPhysLectNotes.53)* **53** (2022) 1 [[arXiv:2109.02696](https://arxiv.org/abs/2109.02696)] [[INSPIRE](https://inspirehep.net)].

[4] PLANCK collaboration, *Planck 2018 results. VI. Cosmological parameters*, *[Astron. Astrophys.](https://doi.org/10.1051/0004-6361/201833910)* **641** (2020) A6 [[arXiv:1807.06209](https://arxiv.org/abs/1807.06209)] [[INSPIRE](https://inspirehep.net)].

[5] SUPERCDMS collaboration, *New Results from the Search for Low-Mass Weakly Interacting Massive Particles with the CDMS Low Ionization Threshold Experiment*, *[Phys. Rev. Lett.](https://doi.org/10.1103/PhysRevLett.116.071301)* **116** (2016) 071301 [[arXiv:1509.02448](https://arxiv.org/abs/1509.02448)] [[INSPIRE](https://inspirehep.net)].

[6] LUX collaboration, *Results on the Spin-Dependent Scattering of Weakly Interacting Massive Particles on Nucleons from the Run 3 Data of the LUX Experiment*, *[Phys. Rev. Lett.](https://doi.org/10.1103/PhysRevLett.116.161302)* **116** (2016) 161302 [[arXiv:1602.03489](https://arxiv.org/abs/1602.03489)] [[INSPIRE](https://inspirehep.net)].

[7] PANDAX-II collaboration, *Dark Matter Results From 54-Ton-Day Exposure of PandaX-II Experiment*, *[Phys. Rev. Lett.](https://doi.org/10.1103/PhysRevLett.119.181302)* **119** (2017) 181302 [[arXiv:1708.06917](https://arxiv.org/abs/1708.06917)] [[INSPIRE](https://inspirehep.net)].

[8] DARKSIDE collaboration, *Low-Mass Dark Matter Search with the DarkSide-50 Experiment*, *[Phys. Rev. Lett.](https://doi.org/10.1103/PhysRevLett.121.081307)* **121** (2018) 081307 [[arXiv:1802.06994](https://arxiv.org/abs/1802.06994)] [[INSPIRE](https://inspirehep.net)].

[9] XMASS collaboration, *A direct dark matter search in XMASS-I*, *[Phys. Lett. B](https://doi.org/10.1016/j.physletb.2018.10.070)* **789** (2019) 45 [[arXiv:1804.02180](https://arxiv.org/abs/1804.02180)] [[INSPIRE](https://inspirehep.net)].

[10] XENON collaboration, *Dark Matter Search Results from a One Ton-Year Exposure of XENON1T*, *[Phys. Rev. Lett.](https://doi.org/10.1103/PhysRevLett.121.111302)* **121** (2018) 111302 [[arXiv:1805.12562](https://arxiv.org/abs/1805.12562)] [[INSPIRE](https://inspirehep.net)].

[11] EDELWEISS collaboration, *Searching for low-mass dark matter particles with a massive Ge bolometer operated above-ground*, *[Phys. Rev. D](https://doi.org/10.1103/PhysRevD.99.082003)* **99** (2019) 082003 [[arXiv:1901.03588](https://arxiv.org/abs/1901.03588)] [[INSPIRE](https://inspirehep.net)].

[12] J. Amaré et al., *First Results on Dark Matter Annual Modulation from the ANAIS-112 Experiment*, *[Phys. Rev. Lett.](https://doi.org/10.1103/PhysRevLett.123.031301)* **123** (2019) 031301 [[arXiv:1903.03973](https://arxiv.org/abs/1903.03973)] [[INSPIRE](https://inspirehep.net)].

[13] CRESST collaboration, *First results from the CRESST-III low-mass dark matter program*, *[Phys. Rev. D](https://doi.org/10.1103/PhysRevD.100.102002)* **100** (2019) 102002 [[arXiv:1904.00498](https://arxiv.org/abs/1904.00498)] [[INSPIRE](https://inspirehep.net)].

[14] CDEX collaboration, *Constraints on Spin-Independent Nucleus Scattering with sub-GeV Weakly Interacting Massive Particle Dark Matter from the CDEX-1B Experiment at the China Jinping Underground Laboratory*, *[Phys. Rev. Lett.](https://doi.org/10.1103/PhysRevLett.123.161301)* **123** (2019) 161301 [[arXiv:1905.00354](https://arxiv.org/abs/1905.00354)] [[INSPIRE](https://inspirehep.net)].

[15] G. Adhikari et al., *An experiment to search for dark-matter interactions using sodium iodide detectors*, *[Nature](https://doi.org/10.1038/s41586-018-0739-1)* **564** (2018) 83 [[arXiv:1906.01791](https://arxiv.org/abs/1906.01791)] [[INSPIRE](https://inspirehep.net)].

[16] PANDAX-4T collaboration, *Dark Matter Search Results from the PandaX-4T Commissioning Run*, *Phys. Rev. Lett.* **127** (2021) 261802 [`arXiv:2107.13438`] [InSPIRE].

[17] DEAP collaboration, *First Direct Detection Constraints on Planck-Scale Mass Dark Matter with Multiple-Scatter Signatures Using the DEAP-3600 Detector*, *Phys. Rev. Lett.* **128** (2022) 011801 [`arXiv:2108.09405`] [InSPIRE].

[18] M. Schumann, *Direct Detection of WIMP Dark Matter: Concepts and Status*, *J. Phys. G* **46** (2019) 103003 [`arXiv:1903.03026`] [InSPIRE].

[19] E. Del Nobile, *The Theory of Direct Dark Matter Detection: A Guide to Computations*, `arXiv:2104.12785` [InSPIRE].

[20] J. Cooley, *Dark Matter direct detection of classical WIMPs*, *SciPost Phys. Lect. Notes* **55** (2022) 1 [`arXiv:2110.02359`] [InSPIRE].

[21] J. Aalbers et al., *A next-generation liquid xenon observatory for dark matter and neutrino physics*, *J. Phys. G* **50** (2023) 013001 [`arXiv:2203.02309`] [InSPIRE].

[22] M. Battaglieri et al., *US Cosmic Visions: New Ideas in Dark Matter 2017: Community Report*, in *U.S. Cosmic Visions: New Ideas in Dark Matter*, (2017) [`arXiv:1707.04591`] [InSPIRE].

[23] Y. Kahn and T. Lin, *Searches for light dark matter using condensed matter systems*, *Rept. Prog. Phys.* **85** (2022) 066901 [`arXiv:2108.03239`] [InSPIRE].

[24] A. Mitridate, T. Trickle, Z. Zhang and K.M. Zurek, *Snowmass White Paper: Light Dark Matter Direct Detection at the Interface With Condensed Matter Physics*, in *2022 Snowmass Summer Study*, Seattle U.S.A., July 17–26 2022 [`arXiv:2203.07492`] [InSPIRE].

[25] R. Essig et al., *Snowmass2021 Cosmic Frontier: The landscape of low-threshold dark matter direct detection in the next decade*, in *2022 Snowmass Summer Study*, Seattle U.S.A., July 17–26 2022 [`arXiv:2203.08297`] [InSPIRE].

[26] T. Bringmann and M. Pospelov, *Novel direct detection constraints on light dark matter*, *Phys. Rev. Lett.* **122** (2019) 171801 [`arXiv:1810.10543`] [InSPIRE].

[27] Y. Ema, F. Sala and R. Sato, *Light Dark Matter at Neutrino Experiments*, *Phys. Rev. Lett.* **122** (2019) 181802 [`arXiv:1811.00520`] [InSPIRE].

[28] C.V. Cappiello and J.F. Beacom, *Strong New Limits on Light Dark Matter from Neutrino Experiments*, *Phys. Rev. D* **100** (2019) 103011 [`arXiv:1906.11283`] [InSPIRE].

[29] H. An, M. Pospelov, J. Pradler and A. Ritz, *Directly Detecting MeV-scale Dark Matter via Solar Reflection*, *Phys. Rev. Lett.* **120** (2018) 141801 [`arXiv:1708.03642`] [InSPIRE].

[30] J.-W. Wang, A. Granelli and P. Ullio, *Direct Detection Constraints on Blazar-Boosted Dark Matter*, *Phys. Rev. Lett.* **128** (2022) 221104 [`arXiv:2111.13644`] [InSPIRE].

[31] A. Granelli, P. Ullio and J.-W. Wang, *Blazar-boosted dark matter at Super-Kamiokande*, *JCAP* **07** (2022) 013 [`arXiv:2202.07598`] [InSPIRE].

[32] T. Li and J. Liao, *Electron-target experiment constraints on light dark matter produced in primordial black hole evaporation*, *Phys. Rev. D* **106** (2022) 055043 [`arXiv:2203.14443`] [InSPIRE].

[33] R. Calabrese, M. Chianese, D.F.G. Fiorillo and N. Saviano, *Electron scattering of light new particles from evaporating primordial black holes*, *Phys. Rev. D* **105** (2022) 103024 [`arXiv:2203.17093`] [InSPIRE].

[34] R. Calabrese, M. Chianese, D.F.G. Fiorillo and N. Saviano, *Direct detection of light dark matter from evaporating primordial black holes*, *Phys. Rev. D* **105** (2022) L021302 [`arXiv:2107.13001`] [ɪɴSPIRE].

[35] M. Ibe, W. Nakano, Y. Shoji and K. Suzuki, *Migdal Effect in Dark Matter Direct Detection Experiments*, *JHEP* **03** (2018) 194 [`arXiv:1707.07258`] [ɪɴSPIRE].

[36] M.J. Dolan, F. Kahlhoefer and C. McCabe, *Directly detecting sub-GeV dark matter with electrons from nuclear scattering*, *Phys. Rev. Lett.* **121** (2018) 101801 [`arXiv:1711.09906`] [ɪɴSPIRE].

[37] N.F. Bell, J.B. Dent, J.L. Newstead, S. Sabharwal and T.J. Weiler, *Migdal effect and photon bremsstrahlung in effective field theories of dark matter direct detection and coherent elastic neutrino-nucleus scattering*, *Phys. Rev. D* **101** (2020) 015012 [`arXiv:1905.00046`] [ɪɴSPIRE].

[38] XENON collaboration, *Search for Light Dark Matter Interactions Enhanced by the Migdal Effect or Bremsstrahlung in XENON1T*, *Phys. Rev. Lett.* **123** (2019) 241803 [`arXiv:1907.12771`] [ɪɴSPIRE].

[39] R. Essig, J. Pradler, M. Sholapurkar and T.-T. Yu, *Relation between the Migdal Effect and Dark Matter-Electron Scattering in Isolated Atoms and Semiconductors*, *Phys. Rev. Lett.* **124** (2020) 021801 [`arXiv:1908.10881`] [ɪɴSPIRE].

[40] U.K. Dey, T.N. Maity and T.S. Ray, *Prospects of Migdal Effect in the Explanation of XENON1T Electron Recoil Excess*, *Phys. Lett. B* **811** (2020) 135900 [`arXiv:2006.12529`] [ɪɴSPIRE].

[41] S. Knapen, J. Kozaczuk and T. Lin, *Migdal Effect in Semiconductors*, *Phys. Rev. Lett.* **127** (2021) 081805 [`arXiv:2011.09496`] [ɪɴSPIRE].

[42] N.F. Bell, J.B. Dent, B. Dutta, S. Ghosh, J. Kumar and J.L. Newstead, *Low-mass inelastic dark matter direct detection via the Migdal effect*, *Phys. Rev. D* **104** (2021) 076013 [`arXiv:2103.05890`] [ɪɴSPIRE].

[43] N.F. Bell, J.B. Dent, R.F. Lang, J.L. Newstead and A.C. Ritter, *Observing the Migdal effect from nuclear recoils of neutral particles with liquid xenon and argon detectors*, *Phys. Rev. D* **105** (2022) 096015 [`arXiv:2112.08514`] [ɪɴSPIRE].

[44] S. Chatterjee and R. Laha, *Explorations of pseudo-Dirac dark matter having keV splittings and interacting via transition electric and magnetic dipole moments*, `arXiv:2202.13339` [ɪɴSPIRE].

[45] DᴀʀᴋSɪᴅᴇ collaboration, *Search for dark matter-nucleon interactions via Migdal effect with DarkSide-50*, `arXiv:2207.11967` [ɪɴSPIRE].

[46] J.A. Dror, G. Elor and R. Mcgehee, *Directly Detecting Signals from Absorption of Fermionic Dark Matter*, *Phys. Rev. Lett.* **124** (2020) 18 [`arXiv:1905.12635`] [ɪɴSPIRE].

[47] J.A. Dror, G. Elor and R. Mcgehee, *Absorption of Fermionic Dark Matter by Nuclear Targets*, *JHEP* **02** (2020) 134 [`arXiv:1908.10861`] [ɪɴSPIRE].

[48] J.A. Dror, G. Elor, R. McGehee and T.-T. Yu, *Absorption of sub-MeV fermionic dark matter by electron targets*, *Phys. Rev. D* **103** (2021) 035001 [`arXiv:2011.01940`] [ɪɴSPIRE].

[49] A. Dedes, I. Giomataris, K. Suxho and J.D. Vergados, *Searching for Secluded Dark Matter via Direct Detection of Recoiling Nuclei as well as Low Energy Electrons*, *Nucl. Phys. B* **826** (2010) 148 [`arXiv:0907.0758`] [ɪɴSPIRE].

[50] J. Kopp, V. Niro, T. Schwetz and J. Zupan, *DAMA/LIBRA and leptonically interacting Dark Matter*, *Phys. Rev. D* **80** (2009) 083502 [arXiv:0907.3159] [INSPIRE].

[51] R. Essig, J. Mardon and T. Volansky, *Direct Detection of Sub-GeV Dark Matter*, *Phys. Rev. D* **85** (2012) 076007 [arXiv:1108.5383] [INSPIRE].

[52] P.W. Graham, D.E. Kaplan, S. Rajendran and M.T. Walters, *Semiconductor Probes of Light Dark Matter*, *Phys. Dark Univ.* **1** (2012) 32 [arXiv:1203.2531] [INSPIRE].

[53] R. Essig, A. Manalaysay, J. Mardon, P. Sorensen and T. Volansky, *First Direct Detection Limits on sub-GeV Dark Matter from XENON10*, *Phys. Rev. Lett.* **109** (2012) 021301 [arXiv:1206.2644] [INSPIRE].

[54] S.K. Lee, M. Lisanti, S. Mishra-Sharma and B.R. Safdi, *Modulation Effects in Dark Matter-Electron Scattering Experiments*, *Phys. Rev. D* **92** (2015) 083517 [arXiv:1508.07361] [INSPIRE].

[55] R. Essig, M. Fernandez-Serra, J. Mardon, A. Soto, T. Volansky and T.-T. Yu, *Direct Detection of sub-GeV Dark Matter with Semiconductor Targets*, *JHEP* **05** (2016) 046 [arXiv:1509.01598] [INSPIRE].

[56] B.M. Roberts, V.A. Dzuba, V.V. Flambaum, M. Pospelov and Y.V. Stadnik, *Dark matter scattering on electrons: Accurate calculations of atomic excitations and implications for the DAMA signal*, *Phys. Rev. D* **93** (2016) 115037 [arXiv:1604.04559] [INSPIRE].

[57] R. Essig, T. Volansky and T.-T. Yu, *New Constraints and Prospects for sub-GeV Dark Matter Scattering off Electrons in Xenon*, *Phys. Rev. D* **96** (2017) 043017 [arXiv:1703.00910] [INSPIRE].

[58] T. Emken, R. Essig, C. Kouvaris and M. Sholapurkar, *Direct Detection of Strongly Interacting Sub-GeV Dark Matter via Electron Recoils*, *JCAP* **09** (2019) 070 [arXiv:1905.06348] [INSPIRE].

[59] R. Catena, T. Emken, N.A. Spaldin and W. Tarantino, *Atomic responses to general dark matter-electron interactions*, *Phys. Rev. Res.* **2** (2020) 033195 [arXiv:1912.08204] [INSPIRE].

[60] I.M. Bloch, A. Caputo, R. Essig, D. Redigolo, M. Sholapurkar and T. Volansky, *Exploring new physics with $O(keV)$ electron recoils in direct detection experiments*, *JHEP* **01** (2021) 178 [arXiv:2006.14521] [INSPIRE].

[61] G. Herrera and A. Ibarra, *Direct detection of non-galactic light dark matter*, *Phys. Lett. B* **820** (2021) 136551 [arXiv:2104.04445] [INSPIRE].

[62] D. Bose, T.N. Maity and T.S. Ray, *Solar constraints on captured electrophilic dark matter*, *Phys. Rev. D* **105** (2022) 123013 [arXiv:2112.08286] [INSPIRE].

[63] XENON collaboration, *Light Dark Matter Search with Ionization Signals in XENON1T*, *Phys. Rev. Lett.* **123** (2019) 251801 [arXiv:1907.11485] [INSPIRE].

[64] SUPERCDMS collaboration, *First Dark Matter Constraints from a SuperCDMS Single-Charge Sensitive Detector*, *Phys. Rev. Lett.* **121** (2018) 051301 [arXiv:1804.10697] [INSPIRE].

[65] DARKSIDE collaboration, *Constraints on Sub-GeV Dark-Matter-Electron Scattering from the DarkSide-50 Experiment*, *Phys. Rev. Lett.* **121** (2018) 111303 [arXiv:1802.06998] [INSPIRE].

[66] DARKSIDE-50 collaboration, *Search for dark matter particle interactions with electron final states with DarkSide-50*, FERMILAB-PUB-22-566-ND-PPD-SCD (2022) [arXiv:2207.11968] [INSPIRE].

[67] DAMIC collaboration, *Constraints on Light Dark Matter Particles Interacting with Electrons from DAMIC at SNOLAB*, *Phys. Rev. Lett.* **123** (2019) 181802 [arXiv:1907.12628] [INSPIRE].

[68] EDELWEISS collaboration, *First germanium-based constraints on sub-MeV Dark Matter with the EDELWEISS experiment*, *Phys. Rev. Lett.* **125** (2020) 141301 [arXiv:2003.01046] [INSPIRE].

[69] SENSEI collaboration, *SENSEI: First Direct-Detection Constraints on sub-GeV Dark Matter from a Surface Run*, *Phys. Rev. Lett.* **121** (2018) 061803 [arXiv:1804.00088] [INSPIRE].

[70] SENSEI collaboration, *SENSEI: Direct-Detection Results on sub-GeV Dark Matter from a New Skipper-CCD*, *Phys. Rev. Lett.* **125** (2020) 171802 [arXiv:2004.11378] [INSPIRE].

[71] PANDAX-II collaboration, *Search for Light Dark Matter-Electron Scatterings in the PandaX-II Experiment*, *Phys. Rev. Lett.* **126** (2021) 211803 [arXiv:2101.07479] [INSPIRE].

[72] A. Hryczuk, E. Karukes, L. Roszkowski and M. Talia, *Impact of uncertainties in the halo velocity profile on direct detection of sub-GeV dark matter*, arXiv:2001.09156 [INSPIRE].

[73] J. Buch, M.A. Buen-Abad, J. Fan and J.S.C. Leung, *Dark Matter Substructure under the Electron Scattering Lamppost*, *Phys. Rev. D* **102** (2020) 083010 [arXiv:2007.13750] [INSPIRE].

[74] A. Radick, A.-M. Taki and T.-T. Yu, *Dependence of Dark Matter-Electron Scattering on the Galactic Dark Matter Velocity Distribution*, *JCAP* **02** (2021) 004 [arXiv:2011.02493] [INSPIRE].

[75] T.N. Maity, T.S. Ray and S. Sarkar, *Halo uncertainties in electron recoil events at direct detection experiments*, *Eur. Phys. J. C* **81** (2021) 1005 [arXiv:2011.12896] [INSPIRE].

[76] S.D.M. White and M.J. Rees, *Core condensation in heavy halos: A Two stage theory for galaxy formation and clusters*, *Mon. Not. Roy. Astron. Soc.* **183** (1978) 341 [INSPIRE].

[77] K. Freeman and J. Bland-Hawthorn, *The New Galaxy: Signatures of its formation*, *Ann. Rev. Astron. Astrophys.* **40** (2002) 487 [astro-ph/0208106] [INSPIRE].

[78] M. Vogelsberger et al., *Properties of galaxies reproduced by a hydrodynamic simulation*, *Nature* **509** (2014) 177 [arXiv:1405.1418] [INSPIRE].

[79] V. Springel et al., *First results from the IllustrisTNG simulations: matter and galaxy clustering*, *Mon. Not. Roy. Astron. Soc.* **475** (2018) 676 [arXiv:1707.03397] [INSPIRE].

[80] R. Feldmann et al., *FIREbox: Simulating galaxies at high dynamic range in a cosmological volume*, arXiv:2205.15325 [INSPIRE].

[81] R.S. Somerville and R. Davé, *Physical Models of Galaxy Formation in a Cosmological Framework*, *Ann. Rev. Astron. Astrophys.* **53** (2015) 51 [arXiv:1412.2712] [INSPIRE].

[82] M. Vogelsberger, F. Marinacci, P. Torrey and E. Puchwein, *Cosmological Simulations of Galaxy Formation*, *Nature Rev. Phys.* **2** (2020) 42 [arXiv:1909.07976] [INSPIRE].

[83] V. Belokurov, D. Erkal, N.W. Evans, S.E. Koposov and A.J. Deason, *Co-formation of the disc and the stellar halo*, *Mon. Not. Roy. Astron. Soc.* **478** (2018) 611.

[84] A. Helmi, C. Babusiaux, H.H. Koppelman, D. Massari, J. Veljanoski and A.G.A. Brown, *The merger that led to the formation of the milky way's inner stellar halo and thick disk*, *Nature* **563** (2018) 85.

[85] R.A. Ibata, G. Gilmore and M.J. Irwin, *A Dwarf satellite galaxy in Sagittarius*, *Nature* **370** (1994) 194 [ɪɴSPIRE].

[86] A. Helmi and S.D.M. White, *Building up the stellar halo of the galaxy*, *Mon. Not. Roy. Astron. Soc.* **307** (1999) 495 [`astro-ph/9901102`] [ɪɴSPIRE].

[87] R. Ibata, M. Irwin, G.F. Lewis and A. Stolte, *Galactic halo substructure in the Sloan Digital Sky Survey: The Ancient tidal stream from the Sagittarius dwarf galaxy*, *Astrophys. J. Lett.* **547** (2001) L133 [`astro-ph/0004255`] [ɪɴSPIRE].

[88] V. Belokurov et al., *An Orphan in the Field of Streams*, *Astrophys. J.* **658** (2007) 337 [`astro-ph/0605705`] [ɪɴSPIRE].

[89] M. Lisanti and D.N. Spergel, *Dark Matter Debris Flows in the Milky Way*, *Phys. Dark Univ.* **1** (2012) 155 [`arXiv:1105.4166`] [ɪɴSPIRE].

[90] G.C. Myeong, N.W. Evans, V. Belokurov, N.C. Amorisco and S. Koposov, *Halo Substructure in the SDSS-Gaia Catalogue : Streams and Clumps*, *Mon. Not. Roy. Astron. Soc.* **475** (2018) 1537 [`arXiv:1712.04071`] [ɪɴSPIRE].

[91] G.C. Myeong, N.W. Evans, V. Belokurov, J.L. Sanders and S.E. Koposov, *Discovery of new retrograde substructures: the shards of ω centauri?*, *Mon. Not. Roy. Astron. Soc.* **478** (2018) 5449.

[92] L. Necib, M. Lisanti and V. Belokurov, *Inferred Evidence For Dark Matter Kinematic Substructure with SDSS-Gaia*, `arXiv:1807.02519` [ɪɴSPIRE].

[93] L. Necib, B. Ostdiek, M. Lisanti, T. Cohen, M. Freytsis and S. Garrison-Kimmel, *Chasing Accreted Structures within Gaia DR2 using Deep Learning*, *Astrophys. J.* **903** (2020) 25 [`arXiv:1907.07681`] [ɪɴSPIRE].

[94] Z. Yuan et al., *Dynamical relics of the ancient galactic halo*, *Astrophys. J.* **891** (2020) 39.

[95] S.S. Lövdal, T. Ruiz-Lara, H.H. Koppelman, T. Matsuno, E. Dodd and A. Helmi, *Substructure in the stellar halo near the Sun. I. Data-driven clustering in integrals-of-motion space*, *Astron. Astrophys.* **665** (2022) A57 [`arXiv:2201.02404`].

[96] T. Ruiz-Lara, T. Matsuno, S.S. Lövdal, A. Helmi, E. Dodd and H.H. Koppelman, *Substructure in the stellar halo near the Sun. II. Characterisation of independent structures*, *Astron. Astrophys.* **665** (2022) A58 [`arXiv:2201.02405`].

[97] E. Dodd et al., *The Gaia DR3 view of dynamical substructure in the stellar halo near the Sun*, *arXiv e-prints* (2022) arXiv:2206.11248 [`arXiv:2206.11248`].

[98] SDSS collaboration, *The Ninth Data Release of the Sloan Digital Sky Survey: First Spectroscopic Data from the SDSS-III Baryon Oscillation Spectroscopic Survey*, *Astrophys. J. Suppl.* **203** (2012) 21 [`arXiv:1207.7137`] [ɪɴSPIRE].

[99] GAIA collaboration, *Gaia Data Release 2: Summary of the contents and survey properties*, *Astron. Astrophys.* **616** (2018) A1 [`arXiv:1804.09365`] [ɪɴSPIRE].

[100] R.P. Naidu et al., *Evidence from the h3 survey that the stellar halo is entirely comprised of substructure*, *Astrophys. J.* **901** (2020) 48.

[101] L.-L. Li and F.-H. Liu, *Energy dependent kinetic freeze-out temperature and transverse flow velocity in high energy collisions*, *Eur. Phys. J. A* **54** (2018) 169 [`arXiv:1809.03881`] [ɪɴSPIRE].

[102] H. Yan et al., *Overview of the LAMOST survey in the first decade*, `arXiv:2203.14300` [ɪɴSPIRE].

[103] J. Diemand et al., *Clumps and streams in the local dark matter distribution*, *Nature* **454** (2008) 735 [arXiv:0805.1244] [INSPIRE].

[104] M. Vogelsberger et al., *Phase-space structure in the local dark matter distribution and its signature in direct detection experiments*, *Mon. Not. Roy. Astron. Soc.* **395** (2009) 797 [arXiv:0812.0362] [INSPIRE].

[105] M. Kuhlen, M. Lisanti and D.N. Spergel, *Direct Detection of Dark Matter Debris Flows*, *Phys. Rev. D* **86** (2012) 063505 [arXiv:1202.0007] [INSPIRE].

[106] M. Kuhlen, M. Vogelsberger and R. Angulo, *Numerical Simulations of the Dark Universe: State of the Art and the Next Decade*, *Phys. Dark Univ.* **1** (2012) 50 [arXiv:1209.5745] [INSPIRE].

[107] L. Necib et al., *Under the Firelight: Stellar Tracers of the Local Dark Matter Velocity Distribution in the Milky Way*, arXiv:1810.12301 [INSPIRE].

[108] C.M. Simpson et al., *Simulating cosmological substructure in the solar neighbourhood*, *Mon. Not. Roy. Astron. Soc.: Letters* **490** (2019) L32.

[109] A. Helmi, *Streams, Substructures, and the Early History of the Milky Way*, *Ann. Rev. Astron. Astrophys.* **58** (2020) 205 [arXiv:2002.04340] [INSPIRE].

[110] L.M. Valenzuela and R.-S. Remus, *A Stream Come True — Connecting tidal tails, shells, streams, and planes with galaxy kinematics and formation history*, arXiv:2208.08443.

[111] V. Belokurov et al., *Energy wrinkles and phase-space folds of the last major merger*, *Mon. Not. Roy. Astron. Soc.* **518** (2023) 6200 [arXiv:2208.11135].

[112] C.W. Purcell, A.R. Zentner and M.-Y. Wang, *Dark Matter Direct Search Rates in Simulations of the Milky Way and Sagittarius Stream*, *JCAP* **08** (2012) 027 [arXiv:1203.6617] [INSPIRE].

[113] M. Lisanti, D.N. Spergel and P. Madau, *Signatures of Kinematic Substructure in the Galactic Stellar Halo*, *Astrophys. J.* **807** (2015) 14 [arXiv:1410.2243] [INSPIRE].

[114] C.A.J. O'Hare, N.W. Evans, C. McCabe, G. Myeong and V. Belokurov, *Velocity substructure from Gaia and direct searches for dark matter*, *Phys. Rev. D* **101** (2020) 023006 [arXiv:1909.04684] [INSPIRE].

[115] M.W. Goodman and E. Witten, *Detectability of Certain Dark Matter Candidates*, *Phys. Rev. D* **31** (1985) 3059 [INSPIRE].

[116] A.K. Drukier, K. Freese and D.N. Spergel, *Detecting Cold Dark Matter Candidates*, *Phys. Rev. D* **33** (1986) 3495 [INSPIRE].

[117] J.D. Vergados and D. Owen, *New velocity distribution for cold dark matter in the context of the Eddington theory*, *Astrophys. J.* **589** (2003) 17 [astro-ph/0203293] [INSPIRE].

[118] A.M. Green, *Effect of realistic astrophysical inputs on the phase and shape of the WIMP annual modulation signal*, *Phys. Rev. D* **68** (2003) 023004 [astro-ph/0304446] [INSPIRE].

[119] F.S. Ling, E. Nezri, E. Athanassoula and R. Teyssier, *Dark Matter Direct Detection Signals inferred from a Cosmological N-body Simulation with Baryons*, *JCAP* **02** (2010) 012 [arXiv:0909.2028] [INSPIRE].

[120] C. McCabe, *The Astrophysical Uncertainties Of Dark Matter Direct Detection Experiments*, *Phys. Rev. D* **82** (2010) 023530 [arXiv:1005.0579] [INSPIRE].

[121] P.J. Fox, J. Liu and N. Weiner, *Integrating Out Astrophysical Uncertainties*, *Phys. Rev. D* **83** (2011) 103514 [arXiv:1011.1915] [ɪɴSPIRE].

[122] P.J. Fox, G.D. Kribs and T.M.P. Tait, *Interpreting Dark Matter Direct Detection Independently of the Local Velocity and Density Distribution*, *Phys. Rev. D* **83** (2011) 034007 [arXiv:1011.1910] [ɪɴSPIRE].

[123] R. Catena and P. Ullio, *The local dark matter phase-space density and impact on WIMP direct detection*, *JCAP* **05** (2012) 005 [arXiv:1111.3556] [ɪɴSPIRE].

[124] A.H.G. Peter, *WIMP astronomy and particle physics with liquid-noble and cryogenic direct-detection experiments*, *Phys. Rev. D* **83** (2011) 125029 [arXiv:1103.5145] [ɪɴSPIRE].

[125] M.T. Frandsen, F. Kahlhoefer, C. McCabe, S. Sarkar and K. Schmidt-Hoberg, *Resolving astrophysical uncertainties in dark matter direct detection*, *JCAP* **01** (2012) 024 [arXiv:1111.0292] [ɪɴSPIRE].

[126] A.M. Green, *Astrophysical uncertainties on direct detection experiments*, *Mod. Phys. Lett. A* **27** (2012) 1230004 [arXiv:1112.0524] [ɪɴSPIRE].

[127] P. Gondolo and G.B. Gelmini, *Halo independent comparison of direct dark matter detection data*, *JCAP* **12** (2012) 015 [arXiv:1202.6359] [ɪɴSPIRE].

[128] E. Del Nobile, G.B. Gelmini, P. Gondolo and J.-H. Huh, *Halo-independent analysis of direct detection data for light WIMPs*, *JCAP* **10** (2013) 026 [arXiv:1304.6183] [ɪɴSPIRE].

[129] Y.-Y. Mao, L.E. Strigari and R.H. Wechsler, *Connecting Direct Dark Matter Detection Experiments to Cosmologically Motivated Halo Models*, *Phys. Rev. D* **89** (2014) 063513 [arXiv:1304.6401] [ɪɴSPIRE].

[130] N. Bozorgnia, R. Catena and T. Schwetz, *Anisotropic dark matter distribution functions and impact on WIMP direct detection*, *JCAP* **12** (2013) 050 [arXiv:1310.0468] [ɪɴSPIRE].

[131] P.J. Fox, Y. Kahn and M. McCullough, *Taking Halo-Independent Dark Matter Methods Out of the Bin*, *JCAP* **10** (2014) 076 [arXiv:1403.6830] [ɪɴSPIRE].

[132] B. Feldstein and F. Kahlhoefer, *A new halo-independent approach to dark matter direct detection analysis*, *JCAP* **08** (2014) 065 [arXiv:1403.4606] [ɪɴSPIRE].

[133] N. Bozorgnia et al., *Simulated Milky Way analogues: implications for dark matter direct searches*, *JCAP* **05** (2016) 024 [arXiv:1601.04707] [ɪɴSPIRE].

[134] G.B. Gelmini, J.-H. Huh and S.J. Witte, *Assessing Compatibility of Direct Detection Data: Halo-Independent Global Likelihood Analyses*, *JCAP* **10** (2016) 029 [arXiv:1607.02445] [ɪɴSPIRE].

[135] R. Laha, *Effect of hydrodynamical-simulation-inspired dark matter velocity profile on directional detection of dark matter*, *Phys. Rev. D* **97** (2018) 043004 [arXiv:1610.08632] [ɪɴSPIRE].

[136] M. Benito, N. Bernal, N. Bozorgnia, F. Calore and F. Iocco, *Particle Dark Matter Constraints: the Effect of Galactic Uncertainties*, *JCAP* **02** (2017) 007 [arXiv:1612.02010] [ɪɴSPIRE].

[137] G.B. Gelmini, J.-H. Huh and S.J. Witte, *Unified Halo-Independent Formalism From Convex Hulls for Direct Dark Matter Searches*, *JCAP* **12** (2017) 039 [arXiv:1707.07019] [ɪɴSPIRE].

[138] A. Ibarra and A. Rappelt, *Optimized velocity distributions for direct dark matter detection*, *JCAP* **08** (2017) 039 [arXiv:1703.09168] [ɪɴSPIRE].

[139] Y. Wu, K. Freese, C. Kelso, P. Stengel and M. Valluri, *Uncertainties in Direct Dark Matter Detection in Light of Gaia's Escape Velocity Measurements*, *JCAP* **10** (2019) 034 [arXiv:1904.04781] [INSPIRE].

[140] N. Bozorgnia and G. Bertone, *Implications of hydrodynamical simulations for the interpretation of direct dark matter searches*, *Int. J. Mod. Phys. A* **32** (2017) 1730016 [arXiv:1705.05853] [INSPIRE].

[141] A. Fowlie, *Halo-independence with quantified maximum entropy at DAMA/LIBRA*, *JCAP* **10** (2017) 002 [arXiv:1708.00181] [INSPIRE].

[142] A. Ibarra, B.J. Kavanagh and A. Rappelt, *Bracketing the impact of astrophysical uncertainties on local dark matter searches*, *JCAP* **12** (2018) 018 [arXiv:1806.08714] [INSPIRE].

[143] J. Herrero-García, Y. Müller and T. Schwetz, *Astrophysics-independent determination of dark matter parameters from two direct detection signals*, *Phys. Dark Univ.* **26** (2019) 100393 [arXiv:1908.07037] [INSPIRE].

[144] N. Bozorgnia et al., *The dark matter component of the Gaia radially anisotropic substructure*, *JCAP* **07** (2020) 036 [arXiv:1910.07536] [INSPIRE].

[145] R. Poole-McKenzie et al., *Informing dark matter direct detection limits with the ARTEMIS simulations*, *JCAP* **11** (2020) 016 [arXiv:2006.15159] [INSPIRE].

[146] G.E. Lawrence, A.R. Duffy, C.A. Blake and P.F. Hopkins, *Gusts in the Headwind: Uncertainties in Direct Dark Matter Detection*, arXiv:2207.07644 [INSPIRE].

[147] G. Gelmini and P. Gondolo, *WIMP annual modulation with opposite phase in Late-Infall halo models*, *Phys. Rev. D* **64** (2001) 023504 [hep-ph/0012315] [INSPIRE].

[148] D. Stiff, L.M. Widrow and J. Frieman, *Signatures of hierarchical clustering in dark matter detection experiments*, *Phys. Rev. D* **64** (2001) 083516 [astro-ph/0106048] [INSPIRE].

[149] K. Freese, P. Gondolo and H.J. Newberg, *Detectability of weakly interacting massive particles in the Sagittarius dwarf tidal stream*, *Phys. Rev. D* **71** (2005) 043516 [astro-ph/0309279] [INSPIRE].

[150] K. Freese, P. Gondolo, H.J. Newberg and M. Lewis, *The effects of the Sagittarius dwarf tidal stream on dark matter detectors*, *Phys. Rev. Lett.* **92** (2004) 111301 [astro-ph/0310334] [INSPIRE].

[151] R. Bernabei et al., *Investigating halo substructures with annual modulation signature*, *Eur. Phys. J. C* **47** (2006) 263 [astro-ph/0604303] [INSPIRE].

[152] C. Savage, K. Freese and P. Gondolo, *Annual Modulation of Dark Matter in the Presence of Streams*, *Phys. Rev. D* **74** (2006) 043531 [astro-ph/0607121] [INSPIRE].

[153] A.H.G. Peter, V. Gluscevic, A.M. Green, B.J. Kavanagh and S.K. Lee, *WIMP physics with ensembles of direct-detection experiments*, *Phys. Dark Univ.* **5–6** (2014) 45 [arXiv:1310.7039] [INSPIRE].

[154] C.A.J. O'Hare, B.J. Kavanagh and A.M. Green, *Time-integrated directional detection of dark matter*, *Phys. Rev. D* **96** (2017) 083011 [arXiv:1708.02959] [INSPIRE].

[155] C.A.J. O'Hare, C. McCabe, N.W. Evans, G. Myeong and V. Belokurov, *Dark matter hurricane: Measuring the S1 stream with dark matter detectors*, *Phys. Rev. D* **98** (2018) 103006 [arXiv:1807.09004] [INSPIRE].

[156] N.W. Evans, C.A.J. O'Hare and C. McCabe, *Refinement of the standard halo model for dark matter searches in light of the Gaia Sausage*, *Phys. Rev. D* **99** (2019) 023012 [arXiv:1810.11468] [INSPIRE].

[157] M.R. Buckley, G. Mohlabeng and C.W. Murphy, *Direct Detection Anomalies in light of Gaia Data*, *Phys. Rev. D* **100** (2019) 055039 [arXiv:1905.05189] [INSPIRE].

[158] A. Ibarra, B.J. Kavanagh and A. Rappelt, *Impact of substructure on local dark matter searches*, *JCAP* **12** (2019) 013 [arXiv:1908.00747] [INSPIRE].

[159] J. Buch, J. Fan and J.S.C. Leung, *Implications of the Gaia Sausage for Dark Matter Nuclear Interactions*, *Phys. Rev. D* **101** (2020) 063026 [arXiv:1910.06356] [INSPIRE].

[160] DEAP collaboration, *Constraints on dark matter-nucleon effective couplings in the presence of kinematically distinct halo substructures using the DEAP-3600 detector*, *Phys. Rev. D* **102** (2020) 082001 [arXiv:2005.14667] [INSPIRE].

[161] X. Ou, L. Necib and A. Frebel, *Robust Clustering of the Local Milky Way Stellar Kinematic Substructures with Gaia eDR3*, arXiv:2208.01056 [INSPIRE].

[162] XENON collaboration, *The Xenon Road to Direct Detection of Dark Matter at LNGS: The XENON Project*, *Universe* **7** (2021) 313 [INSPIRE].

[163] R. Schoenrich, J. Binney and W. Dehnen, *Local Kinematics and the Local Standard of Rest*, *Mon. Not. Roy. Astron. Soc.* **403** (2010) 1829 [arXiv:0912.3693] [INSPIRE].

[164] M. Chen, G.B. Gelmini and V. Takhistov, *Halo-independent analysis of direct dark matter detection through electron scattering*, *JCAP* **12** (2021) 048 [arXiv:2105.08101] [INSPIRE].

[165] C. McCabe, *The Earth's velocity for direct detection experiments*, *JCAP* **02** (2014) 027 [arXiv:1312.1355] [INSPIRE].

[166] B. Holdom, *Two U(1)'s and Epsilon Charge Shifts*, *Phys. Lett. B* **166** (1986) 196 [INSPIRE].

[167] N. Borodatchenkova, D. Choudhury and M. Drees, *Probing MeV dark matter at low-energy e^+e^- colliders*, *Phys. Rev. Lett.* **96** (2006) 141802 [hep-ph/0510147] [INSPIRE].

[168] X. Chu, T. Hambye and M.H.G. Tytgat, *The Four Basic Ways of Creating Dark Matter Through a Portal*, *JCAP* **05** (2012) 034 [arXiv:1112.0493] [INSPIRE].

[169] T. Lin, H.-B. Yu and K.M. Zurek, *On Symmetric and Asymmetric Light Dark Matter*, *Phys. Rev. D* **85** (2012) 063503 [arXiv:1111.0293] [INSPIRE].

[170] E. Izaguirre, G. Krnjaic, P. Schuster and N. Toro, *Analyzing the Discovery Potential for Light Dark Matter*, *Phys. Rev. Lett.* **115** (2015) 251301 [arXiv:1505.00011] [INSPIRE].

[171] J. Alexander et al., *Dark Sectors 2016 Workshop: Community Report*, arXiv:1608.08632 [INSPIRE].

[172] C. Boehm, X. Chu, J.-L. Kuo and J. Pradler, *Scalar dark matter candidates revisited*, *Phys. Rev. D* **103** (2021) 075005 [arXiv:2010.02954] [INSPIRE].

[173] T. Lin, *Sub-GeV dark matter models and direct detection*, *SciPost Phys. Lect. Notes* **43** (2022) 1 [INSPIRE].

[174] https://github.com/tientienyu/QEdark.

[175] A.J. Deason et al., *The local high-velocity tail and the galactic escape speed*, *Mon. Not. Roy. Astron. Soc.* **485** (2019) 3514.

[176] D.B. Zucker et al., *The GALAH survey: No chemical evidence of an extragalactic origin for the nyx stream*, *Astrophys. J. Lett.* **912** (2021) L30.

[177] P. Du, D. Egana-Ugrinovic, R. Essig and M. Sholapurkar, *Sources of Low-Energy Events in Low-Threshold Dark-Matter and Neutrino Detectors*, *Phys. Rev. X* **12** (2022) 011009 [arXiv:2011.13939] [InSPIRE].

[178] R. Essig, M. Sholapurkar and T.-T. Yu, *Solar Neutrinos as a Signal and Background in Direct-Detection Experiments Searching for Sub-GeV Dark Matter With Electron Recoils*, *Phys. Rev. D* **97** (2018) 095029 [arXiv:1801.10159] [InSPIRE].

[179] J. Wyenberg and I.M. Shoemaker, *Mapping the neutrino floor for direct detection experiments based on dark matter-electron scattering*, *Phys. Rev. D* **97** (2018) 115026 [arXiv:1803.08146] [InSPIRE].

[180] T. Schwemberger and T.-T. Yu, *Detecting beyond the standard model interactions of solar neutrinos in low-threshold dark matter detectors*, *Phys. Rev. D* **106** (2022) 015002 [arXiv:2202.01254] [InSPIRE].

[181] J. Billard, L. Strigari and E. Figueroa-Feliciano, *Implication of neutrino backgrounds on the reach of next generation dark matter direct detection experiments*, *Phys. Rev. D* **89** (2014) 023524 [arXiv:1307.5458] [InSPIRE].

[182] C.A.J. O'Hare, *Dark matter astrophysical uncertainties and the neutrino floor*, *Phys. Rev. D* **94** (2016) 063527 [arXiv:1604.03858] [InSPIRE].

[183] G. Cowan, K. Cranmer, E. Gross and O. Vitells, *Asymptotic formulae for likelihood-based tests of new physics*, *Eur. Phys. J. C* **71** (2011) 1554 [arXiv:1007.1727] [InSPIRE].

[184] C.A.J. O'Hare, *Can we overcome the neutrino floor at high masses?*, *Phys. Rev. D* **102** (2020) 063024 [arXiv:2002.07499] [InSPIRE].

[185] J.G. Skellam, *The frequency distribution of the difference between two poisson variates belonging to different populations*, *J. Roy. Statist. Soc.* **109** (1946) 296.